Aalborg Universitet

Indentation deformation in oxide glasses

Quantification, structural changes, and relation to cracking

Januchta, Kacper; Smedskjær, Morten Mattrup

Link to publication from Aalborg University

Indentation deformation in oxide glasses: Quantification, structural changes, and relation to cracking

Kacper Januchta, Morten M. Smedskjaer*

Department of Chemistry and Bioscience, Aalborg University, Aalborg, Denmark

ABSTRACT

Improving the fracture resistance of oxide glasses through adjustment of the chemical composition remains a challenging task, although composition-mechanical property relations have been established for simple model systems. The glass mechanical properties are, among other methods, conventionally tested using instrumented indentation, which is a fast and convenient technique that mimics the real-life damage for certain applications, although interpretation can be challenging due to the complex stress fields that develop under the indenter. Early indentation experiments have shown that oxide glasses exhibit pronounced tendency to densify under compressive load compared to metals and ceramics. After decades of investigations, it is now known that the extent of densification is strongly dependent on the glass' chemical composition and in turn its atomic packing density and Poisson's ratio. Spectroscopic techniques have shed light on the mechanism of densification, which include changes in the bond angle distributions as well as an increase in the coordination number of the network-forming cations. Knowledge of such details is crucial for understanding the link between chemical composition and resistance to cracking in oxide glasses, since densification is an efficient way to dissipate the elastic energy applied to the material during indentation. Here, we review the experimental work on identification and quantification of indentation deformation in glasses, as well as on probing the accompanying structural changes in the glassy network. We also include the conclusions drawn from computer simulation studies, which can provide atomistic details of the indentation deformation mechanisms. Finally, we discuss the link between the mechanism of deformation and the crack resistance.

1. Introduction

Oxide glasses are textbook examples of brittle materials. When subjected to loading, amplification of stresses occurs around surface flaws, leading to catastrophic fracture [1]. Like a puzzle, the two broken glass surfaces can be perfectly reassembled, confirming that no permanent deformation has occurred prior to failure. This is because these iono-covalent materials lack the ability to undergo dislocative motions as those observed in ductile metals. In metals, atoms can easily "jump" to the next neighbor without any permanent damage, which is an efficient way to blunt the tip of the flaw and thus increase the fracture toughness [2]. On the other hand, oxide glasses have been believed to not exhibit any plasticity, at least not on a macroscopic scale. However, already in the late 1940s, it was pointed out that brittle fracture can be avoided when the surface of an oxide glass is permanently deformed by a sharp object, as long as the magnitude of the point load is kept below a given critical value [3–6]. Other studies have implied that glasses are indeed capable of undergoing plastic

deformations based on observations of scratch grooves [7], the mismatch between the fracture surface energy and the energy absorbed during breaking of a glass specimen [8–10], and compaction under high hydrostatic pressures [11,12].

These observations were soon followed by several studies [13–20] on glass indentation (i.e., controlled contact loading) to understand plasticity. Indentation is an attractive technique, since it requires a relatively small sample area, the sample preparation is easy, and the experiment time is short. Indentation also provides information regarding hardness of the material, and when combined with depth-sensing apparatus, elasticity data can also be extracted from the load-displacement curve [21]. In case of oxide glasses and ceramics, indentation is frequently used to evaluate the characteristics and extent of the cracking pattern [22–24]. Based on the length of the cracks emanating from the indentation imprint, various empirical models have been proposed to estimate the fracture toughness of brittle solids [25–27]. However, these attempts have been repeatedly criticized, arguing that the measurements are inconsistent, and the models do not

properly describe the complex indentation stress field and do not take the energy-dissipative deformation processes into account [28–30]. Nevertheless, analysis of indentation cracking is highly relevant for many applications, as the contact with a sharp object is often the process that leads to the formation of a critical flaw. Although not being able to measure fracture toughness, indentation serves as an important tool for studying the damage resistance (e.g., hardness and crack resistance) of different oxide glasses. For example, various studies suggest that the resistance to initiate cracking upon indentation is associated with the ability of a glass to dissipate the supplied mechanical energy through densification facilitated by structural rearrangements [31–35]. However, more understanding is necessary to properly link glass chemistry and network structure with the indentation deformation mechanism and cracking resistance.

The purpose of this paper is thus to provide an overview of the deformation characteristics, structural rearrangements, and the theory behind initiation of cracking associated with indentation in oxide glasses. The main focus is on the existing empirical data on the competing plastic deformations accompanying Vickers indentation (densification and shear flow). The experimental findings presented herein are also supported with relevant contributions from computational studies. The data is evaluated with respect to indentation cracking throughout the paper, as the ultimate aim is to improve the current understanding of deformation mechanisms, which can in turn facilitate design of novel glasses, which are less easily damaged by sharp contact loading.

The review paper is divided into 8 sections. In Section 2, the current state-of-the-art of indentation deformation mechanisms, stress field developed during indentation, and resulting cracking is reviewed. In Section 3, the experimental and computational techniques used to study deformation mechanisms are summarized. In Section 4, the structural changes accompanying densification in different glasses are evaluated. In Section 5, the size and shape of the densified zone as investigated by different probing techniques are reviewed. In Section 6, the dependence of the volumetric ratio of densification and shear flow on the chemical composition, loading rate, indenter geometry, and other aspects are considered. In Section 7, the information gathered in the previous sections is used to shed new light on the correlations between chemical composition, atomic structure, and resistance to indentation cracking. Finally, Section 8 provides some suggestions for future research directions to facilitate better understanding of deformation mechanism during indentation in glasses.

2. Fundamentals of indentation: stress field, deformation, and cracking

2.1. Indentation stress field

When loaded with a relatively blunt object, such as a sphere, glass is likely to deform elastically, as shown by Hertz [36], since the stresses developed during such loading do not reach the yield stress condition. There is thus no cracking, unless the radius of the sphere is sufficiently small, in which case plastic deformation occurs as well. In the case of small radius sphere or when the glass surface is loaded with a sharper object, the response is elastic-plastic [37]. This means that during loading, the glass is permanently displaced through densification and/or shearing (these two mechanisms are discussed in detail in Section 2.2), creating a hemi-spherical zone of compacted material surrounding the indentation cavity [38–40]. A cross-section view of an indenter tip penetrated into the glass surface is schematically illustrated in Fig. 1.

Some of the elastic energy supplied by the indenter tip is spent on the plastic deformation, but the remaining part is recovered through a "spring-back" upon unloading [37]. As the elastic field acts beyond the range of the compacted hemi-sphere, a part of the elastically deformed material is prohibited from recovering. Consequently, the densified zone is under compressive stress, while the elastic zone is under tensile

stress. This can lead to crack initiation at the elastic-plastic boundary [41]. Yoffe [41] performed an elastic-plastic analysis of the indentation problem for a conical indentation, deriving the following expressions for stresses acting in the three-dimensional half-space surrounding the indentation cavity (with Poisson's ratio = 0.25):

$$\sigma_r = \left[\frac{P}{4\pi r^2}\right][1 - 7\cos\theta] + \left[\frac{B}{r^3}\right][19\cos^2\theta - 7], \tag{1}$$

$$\sigma_\theta = \left[\frac{P}{4\pi r^2}\right]\left[\frac{\cos^2\theta}{(1 + \cos\theta)}\right] - \left[\frac{B}{r^3}\right]\cos^2\theta, \tag{2}$$

$$\sigma_\phi = \left[\frac{P}{4\pi r^2}\right]\left[\cos\theta - \left\{\frac{1}{(1 + \cos\theta)}\right\}\right] + \left[\frac{B}{r^3}\right][2 - 3\cos^2\theta], \tag{3}$$

$$\tau_{r\theta} = \left[\frac{P}{4\pi r^2}\right]\left[\frac{\sin\theta\cos\theta}{(1 + \cos\theta)}\right] + \left[\frac{B}{r^3}\right][5\sin\theta\cos\theta], \tag{4}$$

$$\tau_{r\phi} = \tau_{\phi\theta} = 0. \tag{5}$$

Here, the normal and shear stresses (σ and τ, respectively) are expressed in polar coordinates (r, θ, φ), where P is the normal load, and B is the "blister field". The values of P and B control whether the stresses are tensile or compressive. When the stress is tensile, there is a driving force for crack initiation. While P is quite straightforward to understand, B is a less intuitive parameter. This blister field arises from a strain nucleus built on the two forces acting along the surface and the force acting along the vertical axis [34]. The strength of B is difficult to determine given that a part of the elastic energy is dissipated through, e.g., densification, as discussed in Refs. [42, 43]. Sellappan et al. [34] suggested a quantification of the blister field strength for the case of Vickers indentation:

$$B = \frac{3E}{4\pi(1 + \nu)(1 - 2\nu)}(1 - V_R - V_P)V_i^-, \tag{6}$$

where E and ν are Young's modulus and Poisson's ratio of the glass, respectively, V_R is the volume recovery ratio derived from sub-T_g annealing treatment following the method in Ref. [38], V_P is the fraction of pile-up, and V_i^- is the indent cavity volume. The quantification of V_R, V_P, and V_i^- is discussed in detail in Section 3.1. The important information contained in Eq. (6) is that the driving force for indentation cracking is influenced by the extent of energy dissipation, which is in turn correlated with the glass' permanent deformation mechanism.

2.2. Permanent deformation: densification vs. shear flow

The indentation-induced deformation in glass was originally suggested by Taylor [3] to be due to shear flow (the term 'plastic flow' is also frequently used in the literature for the same phenomenon), similar to that observed in ductile materials. Douglas [13] also discussed the possibility to activate cold viscous flow at sufficiently large shear stresses, such as those occurring locally during sharp-contact loading. The claimed observation of shear flow was supported by Marsh [14], who employed rapid indentation as well as indentation in liquid nitrogen to test hardness of different oxide glasses. The fatigue-free hardness number (i.e., that tested in liquid nitrogen) for soda-lime silica glass was found to be much higher than the room-temperature hardness, while the short-time indentation experiment (contact time of $\sim 10^{-5}$ s) led to hardness values approaching the fatigue-free hardness. These observations strongly supported that shear flow is, at least partly, responsible for the deformation during indentation, since hardness depends on both time and temperature.

Peter [20] and later Evers [16] proposed that the glass surface is deformed due to densification as that observed in the high pressure experiments of Bridgman and Simon [11,12]. A significant increase in the refractive index of the glass in the zone beneath the indentation imprint was found by Ernsberger [17], supporting that densification
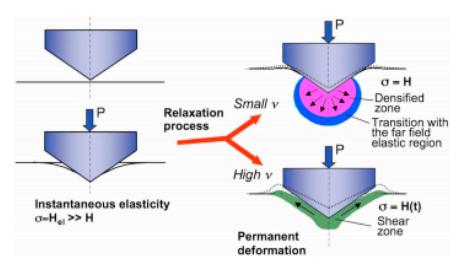
Fig. 1. Schematic representation of the deformation mechanisms occurring during indentation. The indenter is pressed into the surface of the material at a given load (P). Once fully penetrated, the mean contact pressure (σ) corresponds to the instantaneous or elastic hardness (H_{el}), which is significantly larger than the hardness (H) after full recovery. The prevailing deformation mechanism is controlled by the value of Poisson's ratio (ν). Figure reproduced from Rouxel et al. [39] with permission of AIP Publishing.

occurs during contact loading. As opposed to the volume-conservative shear flow discussed by Marsh and others [3,13,14], densification is a process where the atomic network attains a more closely packed arrangement, as shown by infrared spectroscopy [18], but the bonds involved are not necessarily broken. The idea of indentation being associated with densification in oxide glasses is in good agreement with later work of Neely and Mackenzie, showing that part of the deformed zone can be recovered upon thermal annealing using amorphous silica as an example [19]. The activation energy associated with the volume recovery was much less than the energy needed to initiate any viscous flow. Hence, the authors ruled out the possibility of shear or viscous flow being responsible for displacement of the material during indentation, concluding that silica glass deforms through densification.

By studying different glass compositions, Peter [15] showed that the response of oxide glasses to indentation in general includes both densification and shear flow. Scanning electron microscopy (SEM) images of the indented sites allowed Peter to provide visual indication of both deformation mechanisms. The cross-sectional image of a ball indented alkali silicate glass (Fig. 2) sho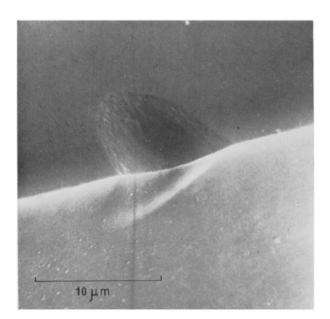ws a clear contrast between the bulk glass and a hemispherical deformation zone beneath the indent site, suggesting densification. On the other hand, inspection of a sharp indentation imprint in the alkali silicate surface reveals that part of the material must have been displaced through shear flow during indentation, as the material is piled up around the indentation imprint above the glass surface (Fig. 3). Besides the pile-up, the observations of shear bands (also called slip lines) suggest that glasses are indeed subject to shearing during indentation [24,44,45]. Shear bands (Fig. 4) are visible as parallel lines or waves moving outwards from the point of contact and are indicative of flow-like material deformation [45]. The preferable deformation mode depends on the chemical composition, with the main criterion for activation of either of the deformation mechanisms being the content of network-modifying oxides [15]. In other words, glasses with high modifier oxide concentration tend to deform through shear flow, while those with lower modifier oxide contents deform primarily through densification. This has later been supported by a quantitative analysis of the two deformation contributions [38], as well through molecular dynamic simulations [46].

2.3. Indentation cracking

The indentation cracking patterns are strongly composition dependent [23,47–49]. For instance, amorphous silica is known to form ring cracks around the indentation imprint [24,50], while soda lime silica has a tendency to form long radial cracks, emanating from the corners of the indent [24,25,51] (Fig. 5). These different cracking systems have been replicated using computational methods [52–54]. The different cracking systems found in oxide glasses are illustrated in Fig. 6 [52]. Arora and co-workers [24] found that the division of glass compositions according to their characteristic cracking pattern (and thus deformation mechanism) is connected with the classification of normal and anomalous composition, as derived from their thermomechanical properties

Fig. 2. Scanning electron microscope image of a ball indentation impression in the surface of an alkali silicate glass along with the cross-section view of the deformation zone beneath the indentation cavity. The clear contrast line beneath the surface indicates the size of the densified zone.
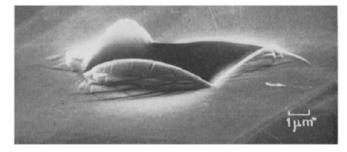Figure reproduced from Peter [15] with permission of Elsevier.

Fig. 3. Scanning electron microscopy image of an indent impression in an alkali silicate glass formed by a 70° pyramidal indenter.
Figure reproduced from Peter [15] with permission of Elsevier.

Fig. 4. Berkovich indent impression in a soda-lime silica glass with highlighted shear bands. The shear bands are indicative of plastic flow and are responsible for serration of the load-displacement curve acquired during the indentation.
Figure reprinted from Chakraborty et al. [45] with permission of Springer Nature.

[18]. The elastic moduli of normal glasses display a negative temperature dependence, but in certain cases the elastic moduli initially increase with increasing temperature [55]. This behavior is referred to as anomalous, and has also been detected in numerous other properties including deformation and fracture, especially for silica glass [19,56,57]. This gave rise to numerous studies focusing on the deformation mechanism, as well as the type and extent of cracking upon sharp contact loading in various oxide glasses [31,34,38,58–62]. Sehgal and Ito [31] demonstrated that the proneness to form cracks upon indentation can be significantly improved by adjusting the chemical composition of the glass. A low packing density facilitating energy dissipation through densification has been proposed to be associated with high resistance against indentation cracking. In other words, the tendency of the so-called "less-brittle" glass studied by Sehgal and Ito to crack is reduced due to the low blister field value, as discussed in Section 2.1. Further advancements in compositional design lead to the discovery of even more crack-resistant glasses [32,35], but there is currently no universal method to accurately predict the crack resistance (defined below). On the other hand, Sellappan et al. [34] showed that based on other mechanical properties (hardness, Young's modulus, and Poisson's ratio), the cracking pattern can be predicted using the stress field calculations of Yoffe [41] (Eqs. (1)–(6)), and a quantitative approximation of the blister field. The driving force for the ring, radial,

median, and lateral cracks (depicted in Fig. 6) can thus be calculated from the following equations according to Ref. [63]:

$$\frac{\sigma_{rr}(r=a, \theta=\pi/2)}{H} = \frac{1-2\nu}{2} + \frac{\gamma\xi(\nu-2)}{(1+\nu)(1-2\nu)\tan\psi}\left[1 - 2(1-\nu^2)\frac{H}{E}\tan\psi\right]^{1/2}\frac{E}{H}, \quad (7)$$

$$\frac{\sigma_{\phi\phi}(r=a, \theta=\pi/2)}{H} = \frac{2\nu-1}{2} + \frac{\gamma\xi}{(1+\nu)\tan\psi}\left[1 - 2(1-\nu^2)\frac{H}{E}\tan\psi\right]^{1/2}\frac{E}{H}, \quad (8)$$

$$\frac{\sigma_{\theta\theta}(r=a, \theta=0)}{H} = \frac{1-2\nu}{2} - \frac{\gamma\xi}{2(1+\nu)\tan\psi}\left[1 - 2(1-\nu^2)\frac{H}{E}\tan\psi\right]^{\frac{1}{2}}\frac{E}{H}, \quad (9)$$

$$\frac{\sigma_{rr}(r=a, \theta=0)}{H} = -\frac{3}{2} + \frac{3\gamma\xi}{(1+\nu)(1-2\nu)\tan\psi}\left[1 - 2(1-\nu^2)\frac{H}{E}\tan\psi\right]^{\frac{1}{2}}\frac{E}{H}. \quad (10)$$

In Eqs. (7)–(10), E, H, and ν are the Young's modulus, hardness and Poisson's ratio of the glass, respectively, ψ is the indenter angle, while γ and ξ are parameters characterizing the elastic recovery upon unloading and the energy dissipation through plastic deformation, respectively:

$$\gamma = \frac{u_t}{u_g}, \quad (11)$$

$$\xi = 1 - V_R - V_P. \quad (12)$$

Here, u_t is the full indenter penetration depth during loading (i.e.,

Fig. 5. The characteristic Vickers cracking patterns seen from top view (top row) and side view at the indent cross sections (bottom row) for soda lime silica (left) and amorphous silica (right). The subsurface damage in soda lime silica glass is linked to its tendency to deform through shear flow, resulting in a median/radial cracking pattern. Amorphous silica exhibits a high tendency to densify during loading, as seen from the deformation zone located beneath the indent cavity. This mode of deformation yields ring (or often referred to as cone) crack morphology.
Figure reproduced from Arora et al. [24] with permission of Elsevier.

Fig. 6. Cracking systems resulting from Vickers indentation found in oxide glasses. Figure reproduced from Lee et al. [52] with permission of Elsevier.

including the elastic contribution), while u_g is the depth of the indenter in contact with the glass surface during loading. Quantification of V_R and V_P is discussed in detail in Section 3.1. Based on these expressions, it is possible to predict the predominant crac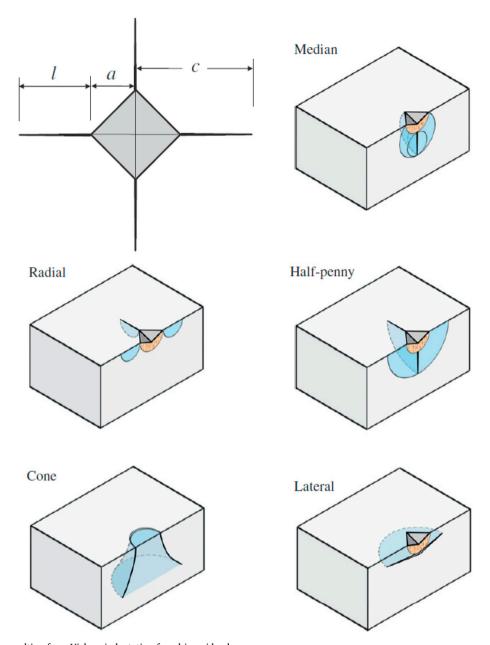king pattern. Glasses with a low ν and low E/H ratios tend to form ring cracks upon indentation, while glasses with high ν and high E/H ratios fracture primarily through radial and lateral cracks. Median cracks predominate in the intermediate region. Hence, it is evident that the deformation behavior influences the crack initiation in oxide glasses.

In order to quantify the damage resistance of different glasses, indentation has been used because it mimics real-life damage for certain applications [64], but also because it is a fast analysis technique that requires little sample preparation. For glasses that exhibit corner cracking, the most common approach is the one suggested by Wada et al. [22], where a Vickers indenter is used to induce a series of imprints at varying load. After unloading, each imprint is evaluated in terms of the amount of radial cracks emanating from its corners. For a given load, the average value of cracks per indent is divided by four

(i.e., the amount of corners per indent and thereby the maximum amount of radial cracks) in order to compute the crack initiation probability at a given load. This is performed at varying loads, starting from low loads responsible for no radial cracking (i.e., 0% crack initiation probability) to high loads leading to extensive cracking (i.e., 100% crack probability). An appropriate mathematical function is then fitted to the data. As illustrated in Fig. 7, the load corresponding to 50% crack probability is defined as indentation cracking resistance, or simply crack resistance (CR).

We note that CR does not describe the resistance to initiation of other types of cracks during sharp contact loading, such as lateral cracks. As such, a more accurate term would be the "critical load for radial crack initiation". It is also important to note that CR not only reflects the glass characteristics, but also the conditions used during the test. Loading rate, bluntness of the tip, time between unloading and recording the cracks, and atmospheric conditions are among the external parameters influencing the proneness of the tested glass to crack [64–66]. Especially the relative humidity plays a major role when
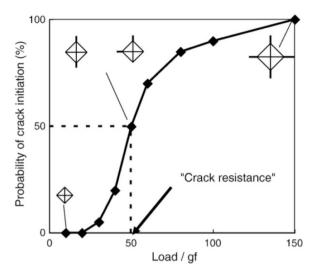
Fig. 7. Schematic representation of crack resistance determination. Figure reproduced from Kato et al. [32] with permission of Elsevier.

Fig. 8. Crack initiation probability as a function of ratio S (Al/(Al + Si)) in calcium aluminosilicate glasses measured in air with ~50% relative humidity (closed symbols) and in N_2 gas (open symbols).
Figure reproduced from Pönitzsch et al. [67] under the Attribution-Non-Commercial-NoDerivatives 4.0 International license (CC BY-NC-ND 4.0).

evaluating *CR* [65]. For instance, a series of calcium aluminosilicate glasses was studied under both ambient atmospheric conditions (~50% RH) and inert N_2 atmosphere [67]. The authors showed that there is an intrinsic compositional trend with respect to the crack initiation probability at 19.6 N load when measured under N_2 atmosphere, while it is not detectable when measured in air since all glasses display 100% crack probability (Fig. 8). The impact of atmospheric water on crack initiation is related to the hydrolysis of the oxide network, which is amplified when the bonds are pre-stressed as it is the case during indentation [56]. This underlines that crack initiation data obtained from different studies should be compared with caution.

2.4. Indentation fracture toughness

Another approach to extract quantitative data from indentation cracking concerns the length of the radial cracks relative to the size of the indent. Lawn and Swain [23] proposed that the measured crack propagation could be related to the fracture toughness (K_{Ic}) by means of fracture mechanics. By collecting data for a few different oxide glasses and ceramics, and calibrating the indentation test values with fracture toughness values obtained from standardized tests, a series of equations [26,27,68,69] to calculate fracture toughness were proposed:

$$K_{Ic} = 0.016(E/H)^{1/2}(P/c^{3/2}), \tag{13}$$

$$K_{Ic} = 0.0309(E/H)^{2/5}(P/c^{3/2}), \tag{14}$$

$$K_{Ic} = 0.0018(E/H)^{1/2}(P/c^{3/2}), \tag{15}$$

$$K_{Ic} = 0.04285/(1 - \nu^2)(HP/l)^{1/2}, \tag{16}$$

$$K_{Ic} = 0.0123(E/H)^{2/5}(HP/l)^{1/2}, \tag{17}$$

where P is the load, c is the radial median crack length, and l is the Palmqvist crack length. All of the above equations relate the elastic and hardness properties as well as the length of the indentation-induced crack (produced at load P) to the fracture toughness through a scaling parameter. The (Eqs. (13)–(15)) apply for a median crack system, i.e., when the cracks emanating from the corners of the indent are originating from the median crack below the point of contact and propagate along the edges to form a half-penny geometry (Fig. 6). On the other hand, (Eqs. (16)–(17)) are used in the case of a Palmqvist crack system, i.e., radial cracks originating from the corners of the indent impression (Fig. 6). While such indentation method to evaluate toughness of ceramic materials continues to be used [70], the application of this method to oxide glasses has received much criticism [28,30,71]. The
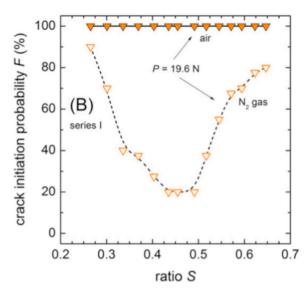
main issue is that the indentation in glass leads to the formation of a complex residual stress field with multiple cracks, which is difficult to describe and quantify [30]. Another important problem is that different toughness values can be calculated from different loads on the same material [30]. Finally, the densification processes that oxide glasses undergo during loading dissipate a part of the supplied work, resulting in a smaller driving force for crack propagation. As a consequence, the indentation fracture toughness does not necessarily only reflect the resistance to crack propagation, but also the proneness to densify. Indentation measurements are thus not believed to be suitable for evaluating the fracture toughness of glasses. Standardized fracture toughness methods such as chevron-notched beam or single-edge precracked beam could be used instead [30,71].

3. Characterization of deformation mechanism

3.1. Microscopy techniques

For micro-indentation, the simplest technique to study indentation-induced deformation is optical microscopy, as important information can be extracted from a qualitative inspection of the indentation-imprint. For instance, the existence of shear faulting lines has been observed [45,72]. The indent is typically imaged with the camera situated normal to the glass surface (from above or below), allowing for rapid evaluation after the indentation. To gain additional insight into the subsurface damage, cross-section views of the indent sites can be investigated. This is done by breaking the glass sample through the diagonal of the indent, following radial cracks emanating from the corners of the indents. That is, an indent is placed next to the tip of an existing scratch or an arrested crack, or a straight line of indents is placed to guide the fracture line, and subsequently the specimen is broken, e.g., by bending [24,73,74].

A frequently used technique to quantify the deformation mechanism is atomic force microscopy (AFM), as suggested in Refs. [38, 75]. This approach consists of recording topographic images of the indent site before and after a thermal treatment at $0.9T_g$ (Fig. 9), which is used to measure how much the indent cavity shrinks upon annealing. This method takes advantage of the different properties of the densified and displaced matter. As pointed out in Ref. [19], densified structures can be recovered by annealing below T_g, and the recoverable volume
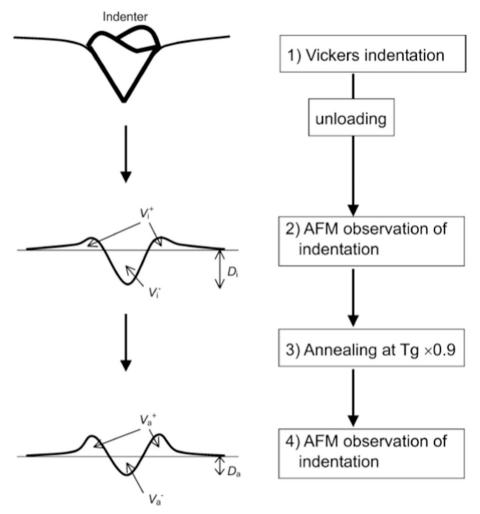
Fig. 9. Schematic representation of the method used to quantify the densification contribution to the total indentation volume. Figure reproduced from Yoshida et al. [38] with permission of Cambridge University Press.

increases with increasing annealing temperature [76]. On the other hand, the volume displaced by shear flow is unaffected by annealing at $0.9T_g$, as the viscosity is too high for any notable viscous flow to occur at the time scale of the experiment (2 h) [77]. We note that the use of $0.9T_g$ as the annealing temperature was based on measurements on a few glass compositions only, mostly limited to silicate glasses [38]. Indeed, the liquid fragility of the composition should be considered when selected the annealing temperature and time to ensure complete relaxation of the densified volume, while avoiding viscous shear flow. The densification volume (V_d) can be calculated by comparing the volumes below and above the surface plane before and after annealing as

$$V_d = (V_i^- - V_a^-) + (V_a^+ - V_i^+), \qquad (18)$$

where the subscripts i and a refer to initial and annealed volumes, respectively, while the superscripts – and + refer to the volumes below and above the glass surface (see Fig. 9). In order to enable comparison among glasses with varying hardness (and thus total indent volumes), V_d is usually normalized with respect to the initial indentation volume, and expressed as the volume recovery ratio (V_R):

$$V_R = V_d/V_i^-. \qquad (19)$$

The remaining volume can result from plastic flow displacement, or alternatively residual elastic strain in or outside the plastic zone. In addition, Sellappan et al. [34] suggested to distinguish between the fraction of plastic flow resulting in the so called pile-up around indent edges (as seen in Fig. 9) and the remaining volume being displaced

downwards or radially away from the indent cavity. This distinction is relevant, as it has been suggested that pile-up dissipates the mechanical work supplied during contact loading, while the remaining volume results in a residual stress, which drives indentation cracking [34]. The fraction of the pile-up volume (V_P) can be extracted from the same topographic measurements as

$$V_P = \frac{2V_i^+ - V_a^+}{V_i^-}. \qquad (20)$$

An approach based on dissolution and AFM measurements has also been proposed to study the extent of densification zone developed during indentation [78,79]. Guin et al. submerged a silicate glass with an indent into a basic aqueous solution, resulting in surface corrosion through hydrolysis. Due to the structural changes induced by indentation, such as the change in the inter-tetrahedral bond angle [80,81], the dissolution rate of the densified zone is higher compared to that of the remaining glass surface. This allows for the visualization of the densified zone by a scanning probe technique, such as AFM.

3.2. Spectroscopic techniques

As densification of the glassy network results in closer packing of the constituent atoms, it is possible to probe the structure of the deformed zone in order to understand the structural rearrangement mechanism and infer the magnitude and extent of densification. Infrared (IR) and Raman spectroscopies are suitable techniques for acquiring

local information about the short- and intermediate-range structure of the glassy network. Both have been employed to probe the structural changes accompanying indentation [61,73], most often using amorphous silica as a simple model glass, for which the IR and Raman spectra are well understood. Furthermore, IR and Raman spectroscopies can also be used to estimate the relative change in density induced by indentation, based on earlier work studying the pressure dependence of the glass structure [82,83]. To do so, a correlation between density and band position (e.g., a characteristic Raman band) is established based on diamond anvil cell (DAC) experiments. This correlation is used to determine the local density in a particular surface spot. Alternatively, the correlation between the location of certain IR bands and the fictive temperature of a glass [84] can be used to shed light on the mechanisms of deformation.

Brillouin spectroscopy has also been used to probe the magnitude of indentation-induced densification following a similar methodology [85], as the longitudinal and transverse sound wave velocities are higher in compressed glasses [82]. By comparing the Brillouin shift to a corresponding density for a given material during a DAC experiment, a calibration curve can be constructed. Then, a measured Brillouin shift acquired from a particular spot in the vicinity of the indentation imprint can be used to calculate the local density. Another approach based on luminescence takes advantage of the pressure-dependence of the electronic transitions occurring in transition metal ions [86]. DAC experiments have shown that the luminescence spectrum of Cr^{3+}-doped silicate glasses changes systematically with increasing density [87]. The change in Cr^{3+}-luminescence within an indent can then be probed using micro-Raman mapping and afterwards converted to a relative change in density. By using either of the techniques discussed above, an indentation-induced densification map can be obtained by compiling the space-resolved spectra, as illustrated in Figs. 10–11.

3.3. Computational techniques

The experimental techniques described above are well supplemented by computational modelling. Finite element analysis of indentation on glass started with the work of Imaoka and Yasui [88,89], involving simulations to reflect the elastic-plastic behavior of glass with densification contribution. Later studies have focused on identifying the appropriate constitutive law to account for the material response to indentation, which is essential for the replication of deformation mechanism through numerical modelling. Von Mises, Mohr-Coulomb, and Drucker-Prager criterions are among the material models employed to understand the indentation deformation [62,90–93]. The current state-of-the-art in finite element analysis of indentation in glass involves the

evaluation of numerical results with respect to the elastic spring-back upon unloading, densification maps, extent of pile-up, and load-displacement curves extracted from experimental indentation cycles.

Cohesive zone finite element modelling [52,54] and discrete element modelling [53,94] are techniques currently used to study the indentation cracking following indentation, and its link to the deformation mechanism. The methodology is similar to the one discussed above, i.e., various material models are considered with respect to their ability to replicate the experimental results. While the predictive power of finite element modelling needs improvement to facilitate detailed studies of deformation and cracking characteristics in different glasses, qualitative trends in, e.g., compositional scaling can be extracted from such studies. Molecular dynamic simulations can also provide insight into the structural origin of deformation mechanism in glasses at the atomic scale. Atomistic models of glassy networks are typically based on parameters defined in force fields such as that of Pedone et al. [95] or BKS [96]. The virtual samples can then be subjected to uniaxial or hydrostatic strains [93,97,98], as well as to indentation [99,100].

4. Structural changes accompanying densification

4.1. Amorphous silica

Amorphous silica is probably the most studied oxide glass in terms of structural changes accompanying densification. Due to the simple chemical composition, only the response of Si−O bonds (neglecting any structural defects) to pressure needs to be accounted for. In modified silicate glasses with additional oxides, the interactions among different cations add an additional degree of complexity. Hence, many studies have focused on silica to gain insights into the structural densification mechanisms, e.g., occurring during indentation [97,101–105].

Sugiura and Yamadaya [82] studied Raman scattering in silica glass subjected to compression. in situ Raman spectra were collected during compression and decompression in a DAC and the changes in the acquired spectra were correlated with those in density. In particular, the so-called D_1 and D_2 bands (located at $\sim490\,cm^{-1}$ and $\sim610\,cm^{-1}$, respectively, in pristine silica) were used as metrics to quantify the extent of densification. The former band is attributed to breathing modes of four-membered rings (i.e., four connected SiO_4 tetrahedral units), while the latter is due to a three-membered ring [106]. The Raman shifts of both D_1 and D_2 increase with increasing density, although that of D_2 is relatively unaffected in the low-pressure regime (up to $\sim2\,GPa$). However, as D_2 does not overlap with the main Raman band of amorphous silica (located at $\sim440\,cm^{-1}$; due to symmetric stretching of Si−O−Si bonds), it is a more convenient measure of the
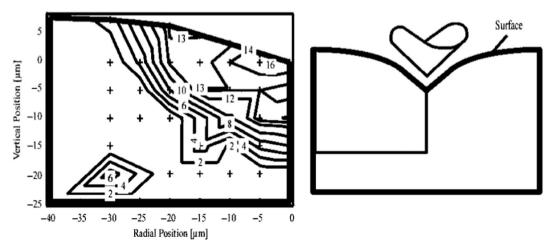

Fig. 10. Raman densification map of Vickers indentation in amorphous silica. The isocontours indicate the relative increase in density. Figure reproduced from Perriot et al. [73] with permission of John Wiley and Sons.
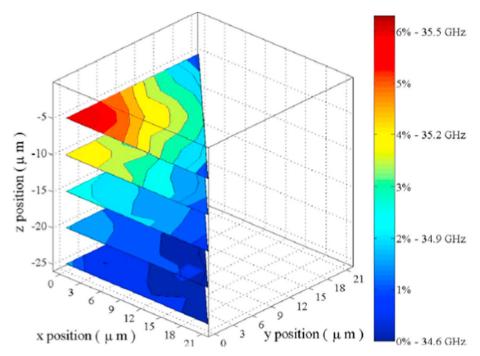
Fig. 11. Densification map of Vickers indent in soda lime silica glass. The local increase in density was determined by space-resolved Brillouin spectroscopy measurements using a density–Brillouin shift calibration curve.
Figure reproduced from Tran et al. [85] with permission of AIP Publishing.

extent of densification. The positions of both D_1 and D_2 lines were also correlated to the fictive temperature of amorphous silica [107,108], and thus also to its density. The finding that light scattering spectra can be associated with density enabled more detailed studies on structural rearrangements accompanying indentation. For example, Perriot et al. [73] probed the extent of the densification zone formed during indentation by monitoring the change in the Raman spectra. Based on this work, the structural changes in amorphous silica induced by indentation involve: i) decrease in the inter-tetrahedral Si—O—Si angle, which is observed through a decrease in the main Raman band (440 cm^{-1}) intensity, and ii) general decrease in free volume observable through an increase in the Raman shifts of the D_1 and D_2 bands (Fig. 12).

The experimentally detected changes in the structure of amorphous silica discussed above are well corroborated by molecular dynamics (MD) simulations. With the pressure-induced increase in density, various studies report decrease in the Si—O—Si angle, redistribution of the ring sizes, reduction of the pore sizes, and overcoordination of Si- and O-atoms [109–111].

4.2. Modified silicate glasses

When modifying oxides such as Na_2O or CaO are added to amorphous silica, the network becomes depolymerized, while the relatively large free volume becomes filled by the modifying cations. This change in the glassy network structure has an impact on the deformation mechanism. Deschamps et al. [81] investigated the structural changes accompanying densification of soda lime silica (window glass). The Raman spectrum of window glass contains more features compared to amorphous silica (Fig. 13). The bands situated at ~450 cm^{-1}, ~560 cm^{-1}, and ~600 cm^{-1} are attributed to stretching of Si—O—Si bonds in Q^4, Q^3, and Q^2 species, respectively [112]. However, the latter may also correspond to the breathing mode of a three-membered ring, as in amorphous silica [106]. In addition, bands at ~950 cm^{-1} and 1100 cm^{-1} are assigned to Si—O stretching modes of Q^2 and Q^3, respectively [81]. The combined indentation and DAC analyses show that the abundance of Q^2 units increases with increasing pressure at the expense of Q^3 units in soda lime silica glass [81,113,114]. On the other

Fig. 12. Raman spectra for pristine (solid line) and indentation-densified (dashed line) amorphous silica. The increase in Raman shift upon indentation of the D_1 and D_2 bands indicates reduction in free volume around the four- and three-membered rings, while the intensity decrease of the main band suggests decreasing inter-tetrahedral Si–O–Si angle.
Figure reproduced from Perriot et al. [73] with permission of John Wiley and Sons.

hand, when Al_2O_3 or B_2O_3 are added to the silicate framework rather than the depolymerizing alkali or alkaline earth oxides, the structural response to indentation resembles that of amorphous silica, i.e., the Raman bands corresponding to three- and four-membered rings appear at higher wavenumbers following the indentation-induced increase in density [113–115]. This indicates that in highly polymerized networks, ring redistribution is the main mechanism facilitating densification, while Q^n reorganization is a primary deformation mode in more modified glasses, usually associated with larger extent of shear flow.

Fig. 13. Raman spectra of soda lime silica glass acquired on the non-indented surface of the glass, and within a 20 N Vickers indent.
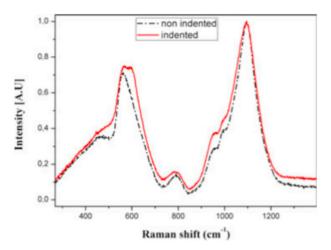Figure reproduced from Kassir-Bodon et al. [120] with permission of John Wiley and Sons.

4.3. Borate glasses

The structural response of borate glasses to indentation-induced densification has received less attention compared to silicate glasses. A study on sodium borate glasses [116] shows that the densification mechanism differs from that of silicate networks, as investigated using Raman spectroscopy in the frequency range from 600 to 900 cm^{-1}. The main bands can be assigned to boroxol rings ($\sim$805 cm^{-1}), BO_4-containing rings such as penta-, tetra- or triborates ($\sim$770 cm^{-1}), and B$-$O$-$B bending vibrations (600–700 cm^{-1}). The 770 cm^{-1} band decreases in intensity upon indentation, but becomes broader. This can be interpreted as a reduction of inter-ring distances, distorting the B$-$O$-$B bridges involving tetrahedral units [116]. The ring statistics also change upon application of pressure, i.e., different superstructures containing BO_4 units are being transformed to others. In aluminoborate glasses, a possible mechanism accompanying densification has been proposed to involve the conversion of triborate rings (containing two BO_3 and one BO_4 unit) into di-triborate rings (containing only one BO_3 and two BO_4 units) [35]. This corresponds to a pressure-induced increase in the average coordination number of boron, in agreement with high pressure inelastic X-ray scattering experiments on amorphous B_2O_3 [117].

5. Evolution of the deformation zone

5.1. Visualization of the deformation zone

The deformation behavior can be studied using optical and scanning electron microscopy. Peter [15] reported excellent images of sharp and ball indentation, providing evidence for the different deformation mechanisms. The contrast between the deformed zone and the bulk is interpreted as densification (Fig. 2), while the pile-up surrounding the edges of the sharp four-sided pyramidal indentation suggests that the glass is at least partly displaced by isochoric shear flow (Fig. 3).

Arora et al. [24] and Hagan [44,50] investigated the origin of the cracking patterns characteristics for silica and soda lime silica glasses. Their image analysis suggested that the cracking behavior is linked to the densification vs. shear flow distribution. Soda lime silica, which tends to deform through shear flow, exhibits severe subsurface damage, while amorphous silica exhibits a densified but non-fractured zone beneath the tip of the indenter (Fig. 5). The images also prove the existence of median/radial and cone cracking systems for soda lime silica and silica glasses, respectively. Normal glasses tend to deform through shear flow, resulting in radial cracks emanating from the corners of the Vickers indent impression, while anomalous glasses tend to easily

densify, resulting in cone cracking. Based on stress field calculations [41], it is possible to deduce the preferred mode of cracking. Poisson's ratio appears to have a large influence on the cracking behavior. Interestingly, Gross [118] found that a so-called intermediate aluminoborosilcate glass (with ν-value exactly at the boundary between anomalous and normal domains) deforms without any subsurface damage (Fig. 14). This manifests itself in higher *CR* compared to soda lime silica and silica glasses. This finding is consistent with the stress field calculations, since this composition should feature limited driving force for the propagation of ring and median/radial cracking [34,63].

Detailed optical and SEM investigations of the indentation impressions in soda lime silica glass, calcium aluminoborosilicate glasses, and amorphous silica have also been performed [45,72,119]. The indent images point to the existence of shear bands formed during indentation in modified glasses (Figs. 4 and 15). Chakraborty et al. [45] noticed that more shear bands are observed when the loading rate is low (i.e., when there is sufficient time for isochoric shear flow to occur). However, the structural origin of the formation of shear bands and their influence on cracking resistance remain poorly understood. Recently, Gross et al. [119] showed that the density of shear bands beneath the point of contact is highly sensitive to changes in chemical composition. Soda lime silica glass with considerable amount of NBOs (expected to facilitate propagation of shear bands) exhibits significant shear bands, with relatively large separation distance. On the other hand, glasses with limited amount of NBOs (e.g., certain calcium aluminoborosilicates) tend to have less prominent shear bands with smaller spacing between them. Furthermore, by changing the composition of these glasses, the proportion between densification and shear flow can be maintained constant, while the shear band density changes (Fig. 15). This has an impact on the driving force for crack initiation, with higher shear band density promoting high resistance to indentation cracking.

5.2. Quantification of the relative density increase

Using in situ high-pressure Raman spectroscopy measurements, Perriot et al. [73] constructed two-dimensional depictions of iso-contours of relative density increase were constructed, as shown in Fig. 10. The maximum density increase is located in the center of the indent, where the compressive stress is assumed to be the largest. For a 2-kgf Vickers indent, the local density increase reaches 16%, which is slightly less than the maximum densification obtained through cold compression at pressures up to $\sim$20 GPa for amorphous silica ($\sim$20%) [105]. The extent of densification decreases with increasing distance from the center of the indent, approaching zero at the edges of the indent impression. The densified zone progresses into the depth of the material, with the extent of densification approaching zero at a depth approximately four times larger than the depth of the indent cavity. The boundary of the densified zone resembles that of a half-penny, in agreement with qualitative microscopic evaluations [15,24,51], finite element modelling [62,90], and discrete element modelling [53]. Similar studies have been performed for a soda lime silica glass [81,120]. Using the pressure-density relation from Ref. [121], and a careful evaluation of the pressure-induced changes in the Raman, a densification map analogous to that of amorphous silica was constructed. Soda lime silica features a significantly smaller maximum extent of densification ($\sim$4%) compared to silica ($\sim$16%), highlighting the difference in deformation mechanism for the two compositions.

Perriot et al. [86] also exploited the density-sensitive luminescence of Cr^{3+}-cations (as detected by Raman spectroscopy) to probe the deformation zone of Cr-doped soda lime silica glass. The extent of densification below the indenter tip extracted using this method was between 3 and 4%. The densification map obtained by Brillouin spectroscopy measurements (Fig. 11) is qualitatively similar to that obtained from Raman studies, although the maximum extent of densification reported is slightly higher (6%) [85].

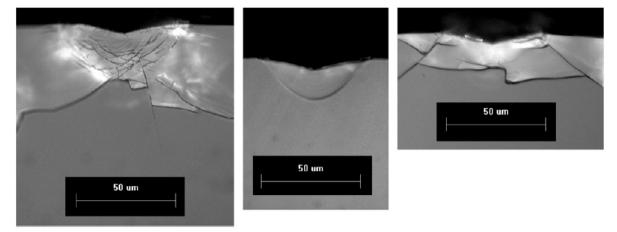An alternative approach to the spectroscopic measurements, which

Fig. 14. Cross-section view of Vickers indentation impressions produced at 1 kgf in the surface of soda lime silica glass (left), intermediate aluminoborosilicate glass (middle), and amorphous silica (right). The transition in the characteristic cracking pattern from median/radial system to ring (cone) cracking morphology follows a decrease in Poisson's ratio. The aluminoborosilicate glass exhibits a Poisson's ratio corresponding to near-zero theoretical driving force for either of the above mentioned cracking modes.
Figure reproduced from Gross [118] with permission of Elsevier.

rely on careful calibration of the spectral response vs. density correlation, is the chemical dissolution technique [78,79]. The structural changes accompanying indentation of silicate glasses appear to enhance the dissolution rate when the glass is exposed to basic aqueous solution. Such increase in the dissolution rate has been found to be quite pronounced in soda lime silica glass, but also measurable in amorphous silica [78]. Using this approach, the topography of the indentation site could be monitored as a function of time using AFM, discovering a hemispherical zone of densified material surrounding the indentation site. This result is in agreement with the spectroscopic mapping techniques [73,120], finite element simulations [52,54,62], discrete element simulations [53], as well as molecular dynamic simulations [93].

6. Deformation mechanism: influence of material characteristics and experimental conditions

6.1. Role of Poisson's ratio

The densification contribution to indentation deformation (as quantified by V_R, see Section 3.1) depends on the glass chemical composition. V_R for amorphous silica exceeds 90%, but the addition of modifying constituents to the glassy network reduces V_R (~60% for soda lime silica glass) [38]. A bulk metallic glass, such as Pd-Ni-P, exhibits practically no volume recovery upon annealing (~5%) [38]. To understand this dependence on glass chemistry, the measured V_R values have been correlated with Poisson's ratio (ν) of the glasses, revealing a decrease of V_R with increasing ν (Fig. 16) [38]. The correlation between the prevailing deformation mechanism and ν is supported by experimental [39] and numerical [92] studies on glasses that have been subjected to pre-densification. This shows that V_R is not purely composition-dependent, as one can manipulate a given glass' susceptibility to densify through isostatic compression. Although ν is defined as the ratio of transverse contraction over longitudinal extension under loading in the elastic regime, it also appears to relate to the resistance against irreversible volume changes. This may be understood because atomic packing density (C_g) has been reported to scale positively with ν [122], leading to the intuitive result that higher C_g values (and thereby ν) lead to an increased resistance towards volume shrinkage, while lower C_g allows the indenter to penetrate the glass surface by reducing the voids in the glassy network. These correlations also explain why modified silicate glasses, such as common window glass, display lower V_R values compared to amorphous silica. The voids in the silicate network are filled with relatively large modifying atoms such as Na or Ca,
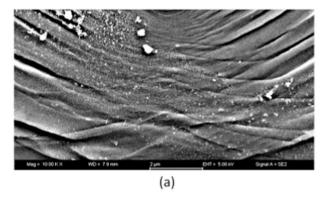
reducing the ability of the network to densify and thus forcing it to deform through a different mechanism.
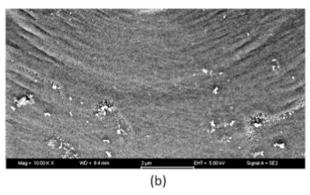
Subsequent studies with more data on different glass systems indicate that there is, however, no one-to-one correlation between V_R and ν nor V_R and C_g [34,123,124], although the overall trend of decreasing V_R with increasing ν does exist. However, in the range of ν from 0.2 to 0.3, glasses with widely different V_R values but similar ν values exist and vice versa. For instance, Scannell et al. [125] found that within the ternary Na_2O-TiO_2-SiO_2 system, the densification contribution to the indentation deformation was constant over a wide range of ν values (0.18–0.23) within the experimental uncertainty, followed by a rapid decrease in V_R with increasing ν at $\nu = 0.24$. It was suggested that other compositional differences, e.g. the evolution of ν, Young's modulus, and hardness with increasing density, come into play. In other words, two glasses with a similar set of material properties can respond differently to indentation if the density dependence of those properties differs. Such changes are composition dependent. Therefore, it is important to consider the nature of the chemical bonds along with ν when estimating V_R. More studies are thus needed to develop a composition dependent model for V_R.

Yoshida's AFM-methodology [38] has also been utilized to understand the correlation between ν and the propensity of glasses to form pile-up around the indentation edges [34]. The formation of pile-up is considered to be related to the ability to activate isochoric shear flow during indentation. Sellappan et al. [34] found that the propensity to form pile-up increases with increasing ν (Fig. 17). For $\nu \sim 0.3$, glasses tend to resist both densification and pile-up formation.

6.2. Role of chemical composition

In order to understand the compositional dependence of deformation mechanism and CR, Kato et al. [33] investigated a series of borosilicate glasses and probed their tendency to densify during indentation. Several SiO_2-rich glass series were investigated, where B_2O_3 was substituted for either SiO_2 or Na_2O. The depth recovery ratio (scaling with V_R) was found to be very sensitive to composition variation. In the $20Na_2O$-xB_2O_3-$(80-x)SiO_2$ system (all fractions in mol%), the indent depth recovery upon annealing displays a minimum at the composition with equal amounts of Na_2O and B_2O_3, i.e., where there is a maximum in the fraction of B in tetrahedral conformation. Upon further addition of B_2O_3, the propensity to densify increases again. This indicates that V_R not only depends on the molar fraction of B_2O_3, but also on its coordination state as controlled by the fractions of the other network
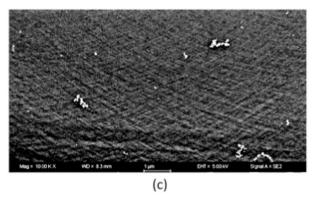
(a)

(b)

(c)

Fig. 15. Cross-sectional SEM images of the subsurface shear bands observed in calcium aluminoborosilicate glasses. Increasing the B_2O_3/SiO_2 ratio (from a to c) leads to an increase in the shear band density.
Figure reproduced from Gross et al. [119] with permission of Elsevier.

Fig. 16. Dependence of Poisson's ratio (ν) on the volume recovery ratio (V_R) for a range of different glasses. The dashed sigmoidal line is a guide for the eye. The data suggests that the propensity to densify when subjected to loading decreases with increasing Poisson's ratio, with the mode of deformation changing from densification to isochoric shear flow.
Figure reproduced from Yoshida et al. [38] with permission of Cambridge University Press.

Fig. 17. Pile-up contribution to the total indentation volume (V_P) as a function of Poisson's ratio (ν) for different glasses. The ability to deform through isochoric shear flow moving towards the edges of the indentation site increases with increasing ν.
Figure reproduced from Sellappan et al. [34] with permission of Elsevier.

constituents. Based on this result, densification was proposed to be facilitated by the open, planar trigonal boron units [33].

The role of boron on V_R was further investigated for xNa$_2$O-(100-x) B$_2$O$_3$ glasses [116]. Initially, when the modifier concentration is low, the network consists primarily of planar boroxol rings, exhibiting a high propensity for shear flow, since the rings are suggested to slide on top of each other. The network becomes more rigid at higher Na$_2$O content, hindering deformation through shear flow and thus manifesting itself as a small increase in V_R. Finally, once the Na$_2$O/B$_2$O$_3$ becomes large enough, i.e., when non-bridging oxygens (NBOs) start to form at the expense of boron tetrahedra, the possibility to shear is enabled, resulting in a decrease in V_R. It is also worth noting that for the binary sodium borate glasses, neither the relation between V_R and ν nor that between V_R and C_g resemble those discussed in Section 6.1. This underlines that the deformation mechanism is sensitive to specific structural units in the glass, and not merely to ν or C_g.

The effect of NBOs on the shear flow deformation has also been investigated in different alkali and alkaline earth silicate glasses [126].
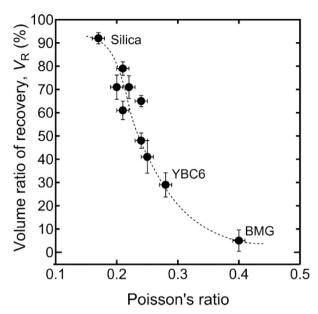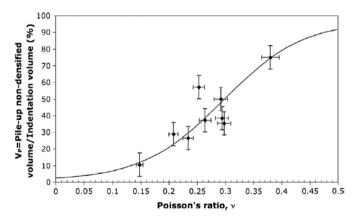
The tendency to deform through densification or shear flow was found to mostly depend on the SiO$_2$ concentration (decreasing V_R with increasing R$_2$O/SiO$_2$ or RO/SiO$_2$ ratio), while the type of modifier or its size has a negligible impact on the V_R value. The ability to shear approaches zero around and below the composition with 80 mol% SiO$_2$. This corresponds to the point where modifier-rich domains, or so-called modifier channels, begin to form according to the modified random network model [127]. These conclusions have been supported by MD simulations on silicate glasses with varying sodium content, where the volumetric strain as a function of hydrostatic pressure was monitored [93]. The shear strength was found to be larger for glasses with higher connectivity, whereas more-depolymerized glasses tend to deform through shear flow at relatively low stresses.

Kjeldsen et al. [128,129] have studied the impact of mixing two different modifier species on the deformation mechanism. Both in

mixed alkali and mixed alkaline earth aluminosilicate glasses, the densified volume displays a local minimum around the composition with equal molar concentrations of the two modifiers, exhibiting the so-called mixed modifier effect. On the other hand, the volume displaced through isochoric shear flow exhibits negative and positive deviation from linearity for alkali and alkaline earth modifiers, respectively. These compositional trends in deformation mechanism correspond well to those observed in hardness, suggesting that the propensity to displace the material through shear flow (i.e., the deformation mechanism with the largest resistance to loading) dictates the value of hardness. These conclusions were later supported by MD simulations [98].

Limbach et al. [123] as well as Barlet et al. [130] have focused on the effect of mixing two network formers (SiO_2 and B_2O_3) on indentation deformation, thereby revisiting the study of Kato et al. [33] on ternary sodium borosilicate glasses. Limbach et al. [123] detected a local minimum in V_R in the ternary sodium borosilicate phase diagram in the vicinity of the $10Na_2O-16B_2O_3-74SiO_2$ composition (Fig. 18), but interestingly, this glass exhibits a fairly low ν-value (0.206). The low ν-value may be attributed to the expected high population of Si- and B-containing reedmergnerite and/or danburite rings [131], which form a rigid three-dimensional network. These superstructures should hinder the propensity to deform through shear, and the authors acknowledge that the low V_R value is in contradiction to the expectations, while suggesting that the current empirical structural models might need to be reconsidered. The contribution of Barlet et al. [130] shows that the densification ability decreases with increasing Na_2O content (and with increasing ν following the Na-induced depolymerization), but the rate of V_R decrease with increasing ν is dictated by the SiO_2/B_2O_3 ratio as illustrated in Fig. 19. This further challenges validity of the V_R vs. ν correlation suggested in Refs. [34, 38].

The structural dependence of V_R has also been studied in the $25Na_2O-xAl_2O_3-(75-x)B_2O_3$ system [124]. In this system, the propensity to densify upon indentation appears to increase slightly towards the metaluminous composition (i.e., with equal Na_2O and Al_2O_3 contents), and then decreases upon further addition of Al_2O_3 to the network. This compositional scaling is interpreted in terms of the boron coordination change as a function of the Al_2O_3/B_2O_3 ratio. Since Na-cations preferentially charge-balances Al-tetrahedra units relative to B-tetrahedra [124,132], the average boron coordination number decreases with increasing Al_2O_3/B_2O_3 ratio. Supplemental hot compression experiments performed on these glasses have shown that boron undergoes a three- to four-coordinated transition with increasing density, which suggests that an increase in coordination may be occurring during indentation [124]. This densification-induced structural reorganization should be most prominent in the glasses with the lowest N_4-values (ratio of four-coordinated to total boron), thus explaining the increase in V_R with increasing Al_2O_3/B_2O_3. Upon crossing the metaluminous border, five-coordinated Al-species begin to form, inducing a decrease in V_R.

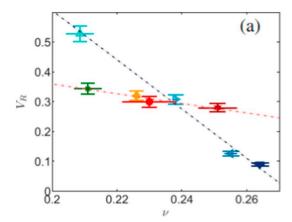**Fig. 19.** Volume recovery ratio (V_R) as a function of Poisson's ratio (ν) for sodium borosilicate glasses. The two dashed lines correspond to two different K-values (SiO_2/B_2O_3 ratios). Glasses with low K-value (~2.5, blue dashed line) line exhibit a higher decrease in V_R with increasing ν compared to glasses with high K (~4.5, red dashed line).
Figure reproduced from Barlet et al. [130] with permission of Elsevier.

6.3. Role of post-treatment

The structure and properties of oxide glasses are dictated by their chemical composition, but can also be tuned by various post-treatment methods. For instance, it is well-known that the thermal history of the glass has a significant impact on its properties. Slowly cooled glasses (i.e., with a lower fictive temperature, T_f) attain a higher density (with the exception of the anomalous SiO_2 [57]), since the glassy network had more time to rearrange its structure corresponding to that of the supercooled liquid at a relatively low temperature. More rapidly cooled glasses with higher T_f has less time available for structural rearrangement, resulting in a structure corresponding to a supercooled liquid at a relatively high temperature with lower density. Intuitively a significant density change is expected to affect the potential to densify during indentation. This has been investigated in several studies outlined in the following.

The indentation cracking and deformation characteristics were studied on an aluminosilicate glass composition subjected to sub-T_g annealing treatment for various durations [133]. The glass sample with the highest T_f (i.e., lowest density) indeed recovers most of its depth upon post-indentation annealing (corresponding to highest V_R), and the tendency to densify during indentation decreases with decreasing T_f. Furthermore, the resistance to indentation cracking was observed to decrease along with the decrease in T_f, which corresponds well with the idea that densification facilitates stress dissipation, minimizing the
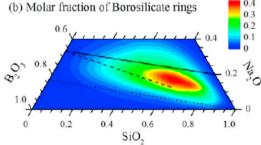

Fig. 18. Representation of the volume recovery ratio (V_R) dependence on the chemical composition in the ternary $Na_2O-B_2O_3-SiO_2$ system. The local minimum corresponds to the expected local maximum in borosilicate rings such as reedmergnerites and danburites.
Figure reproduced from Limbach et al. [123] under the Creative Commons Attribution 4.0 International Public License.

residual stress available for crack initiation. Similar conclusions were reached by Malchow et al. [134], who studied a sodium borosilicate composition. Quenched glass samples exhibited higher tendency to densify during indentation and higher *CR* compared with a slowly cooled sample. Zehnder et al. [135] later investigated the same glass composition and studied the indentation behavior of samples quenched onto graphite molds with varying temperature. An increase in quenching rate (and thus T_f) was found to affect *CR*, in agreement with the work of Malchow et al. [134]. However, it was pointed out that the crack probability vs. indentation load curves were not significantly different for glasses quenched onto molds at 450 °C, 250 °C, or room temperature. In other words, there is a limit for how much *CR* can be improved by increasing T_f.

Rouxel et al. [39] probed the indentation morphology in different inorganic glasses, including amorphous silica, window glass, $GeSe_4$ glass, and $Zr_{55}Cu_{30}Ni_{10}Al_5$ bulk metallic glass. Each glass was subjected to high pressure in a DAC, and the indentation characteristics of the as-made and compressed samples were then compared. Both of the studied oxide glasses exhibited significant increases in density and ν, resulting in higher propensity for pile-up formation (Fig. 20) and decreased tendency for densification. Later, Aakermann et al. [136] subjected a series of aluminosilicate glasses to high-temperature compression, resulting in permanent densification of bulk specimens. Based on quantification of V_R, the compressed glasses are found to be much less prone to densify during indentation compared to the as-made glasses. This was in turn used as an explanation for the pressure-induced decrease in *CR*, since the reduced potential for densification leads to less dissipation of the work supplied by the indenter. The pressure-induced increase in density and accompanying decrease in *CR* has been observed in numerous oxide glass systems [137], with one notable exception. In a modifier-free B_2O_3-P_2O_5-Al_2O_3-SiO_2 composition, compression leads to network densification, but *CR* increases, while V_R is constant within the error range [138]. This underlines the importance of considering the atomic structure of the glass when evaluating the correlation between chemical composition and *CR*.

To the authors' knowledge, there are no published experimental studies of the indentation deformation mechanism of ion-exchanged glasses, which quantify the deformation volumes. However, MD simulations have been used to address this problem. Luo et al. [100] investigated different surface strengthening methods and their impact on the indentation densification, shear deformation, and stress field. Thermal tempering, which is a frequently used method to physically strengthen glass, results in a compressive stress layer at the surface induced by rapid cooling. Ion exchange has the same effect, but occurs due to the replacement of smaller mobile ions in the glass with larger ones from a molten salt bath. In both cases, the compressive stress layer is responsible for inhibition of crack propagation, but the free volume in the affected surface layers of the thermally tempered and ion-exchanged glasses differs. Upon thermal tempering, the glass exhibits higher free volume compared, while the opposite is found for ion-exchanged glasses. This results in a higher propensity to densify during indentation for thermally tempered glasses, and lower densification ability for ion exchanged glasses. These MD simulation results largely agree with experimental studies by Koike et al. [139] as well as Gross and Price [64], who focus on the stress-induced optical retardation. A large change in optical retardation occurs following thermal tempering, which can be interpreted as a shift in deformation mechanism from shear- to densification-driven. However, the impact of chemical strengthening on the optical retardation is significantly smaller and thus more challenging to interpret.

6.4. Role of strain rate

The nanohardness of soda-lime silica glass has been determined using different loading rates [45,140], with a remarkable observation concerning shear bands. That is, the formation of shear bands inside the indent cavity appeared to be rate-dependent. Lower loading rate resulted in a higher concentration of shear bands (Fig. 4), corresponding to highly serrated pattern in the load-displacement curves. Intuitively, this is explained by the longer time available during the slow indentation to activate shear band formation.

Later, Limbach et al. [141] investigated the strain rate sensitivity of

Fig. 20. Topographic images of indentation sites acquired using atomic force microscopy for (a) amorphous silica, (b) amorphous silica compressed at 25 GPa, (c) bulk metallic glass, and (d) platinum. The images suggest that upon pressure treatment, the deformation mechanism for silica glass changes from being densification-dominated to shear-driven, resembling that of highly packed metals.

Figure reproduced from Rouxel et al. [39] with permission of AIP Publishing.

hardness (i.e., dependence of hardness on the loading rate) for a wide range of different glass systems. While no evaluation of densification or shear flow contributions to the indent sites was performed, the study presents valuable information since hardness is linked to the deformation mechanisms. No correlation between the packing density (used as a metric for densification potential by the authors) nor the average bond strength and strain rate sensitivity was found. On the other hand, Poisson's ratio appeared to be a good indicator of the glasses' strain rate sensitivity. For low ν-values and thus high network dimensionality (e.g., amorphous silica), it is assumed that deformation proceeds once an activation barrier is overcome. For intermediate network dimensionality (ν between 0.30 and 0.35), the deformation is highly strain rate-dependent. For sufficiently high ν-values, deformation proceeds independently of the loading rate, while the shear plane is found.

Shikimaka et al. [142] used the AFM method to study the densification contribution to the indentation volume at different strain rates for a series of aluminophosphate glasses. A negative correlation between densification contribution and strain rate was established, which is ascribed to the fact that shear flow is more easily activated when sufficient time for such event is available (i.e., when the strain rate is low). Hardness was also found to decrease with decreasing strain rate [135,142], implying that the rearrangement processes accompanying indentation occur more easily in low strain rate conditions. As more time is available for shearing, and thus for the densified material to be displaced from the indenter tip, further densification is enabled. This is supported by Mackenzie [18], who suggested that shear deformation facilitates densification. In Ref. [142], the authors also examined the load dependence of the deformation mechanism, concluding that the densification contribution decreases with increasing load, in agreement with experimental evidence [143]. This is also a consequence of shear flow being more easily activated when the deformation volume is large.

The above mentioned strain rate dependence of the two deformation mechanisms, shear flow and densification, has also been confirmed by Gross and Price [64] for borosilicate and boroaluminosilicate glasses under dynamic and quasi-static indentation configurations. The difference in deformation mechanisms corresponded well with the strain rate dependence of *CR*, with less subsurface damage leading to less residual stress and thus higher *CR* for shorter contact times.

6.5. Role of indenter geometry

Peter [15] discovered that increasing the indenter tip sharpness leads to more pronounced shear deformation and less densification. This observation was later quantified [144], by using different indenter geometries and measuring the densification contribution to the indentation response of soda lime silica glass. These findings have also been confirmed by microindentation experiments on different oxide glasses [118], nanoindentation experiments on soda lime silica [145], and molecular dynamic simulations for a series of sodium potassium aluminosilicate glasses [99]. Furthermore, Gross [118] observed that the cracking pattern changes from radial/median to ring cracking with increasing indenter angle, which is correlated to the change in the stress field surrounding the indentation cavity, in agreement with the predictions of Yoffe [41].

The correlation between cracking and densification has also been investigated using finite element modelling [54]. The crack length was found to be less sensitive to changes in load for blunter indenters (e.g., Berkovich geometry) compared to sharper indenters (e.g., cube corner geometry). In other words, when the densification is the prevailing deformation mechanism, there is a smaller increase in crack length with increasing load. It was concluded that the Hoop stress is reduced by densification, which forces cracking to initiate at larger depths.

Yoshida et al. [66,146] studied the deformation of various silicate glasses in situ during indentation by situating the indenter on top of an inverted microscope. This enables monitoring the contact area between the glass sample and the indenter tip continuously as the indentation

cycle progresses. These measurements confirmed the above mentioned correlation between indenter sharpness and densification propensity. Additionally, the study also quantified the bowing in of the glass along the edges of the indenter, providing new insight into the deformation behavior. That is, the bow-in parameter, expressed as the ratio between center to corner distance and center to edge distance (L_C/L_F), decreases with increasing sharpness of the indenter (Fig. 21). The bowing in of the glass along the edges was in turn correlated to the event of edge cracking, with larger L_C/L_F ratio corresponding to larger propensity for edge cracking.

7. Reevaluation of densification and cracking data

7.1. Impact of adaptivity on densification contribution

Based on the initial empirical evidence [38] and the correlation between network dimensionality and ν [122], the propensity for glass densification during indentation (V_R) was assumed to scale inversely with ν. However, later work [34,123,124,130] showed that there is considerably more scatter in the V_R vs. ν data compared with the initially proposed sigmoidal relation (Fig. 16). Januchta et al. [35] suggested that the ability to densify during loading not only depends on ν, but also on the ability of structural units abundant in the glass to respond to pressure – the so-called "atomic self-adaptivity". For instance, structural units containing three-coordinated boron atoms are very prone to local rearrangements, and facilitate densification [33,147], which is in turn linked to the ability of boron to change its coordination with oxygen from three to four when subjected to pressure [148]. It is therefore expected that highly adaptive glasses rich in trigonal boron may display higher V_R value than that anticipated for a given ν-value. This is illustrated in Fig. 22, where all the available V_R data is plotted as a function of ν, with the data points for borosilicate glasses indexed by the $[B_2^{III}O_3]/([B_2O_3] + [SiO_2])$ ratio [33,34,38,115,116,123,125,126,129,130,136,138,149,150]. The glasses with the highest trigonal B_2O_3 content relative to the sum of total B_2O_3 and SiO_2 (marked by blue) are shifted to the right of the general trend containing mostly silicate, aluminosilicate, and relatively B_2O_3-poor borosilicate glasses or glasses where most boron is in tetrahedral coordination with oxygen (marked by red). This points to the importance of considering the chemical composition and underlying network structure when predicting V_R.

Fig. 21. Bow-in parameter (L_C/L_F) as a function of the indenter face angle (β) for soda-lime silica glass. The distances corresponding to L_C and L_F, respectively, and the angle β are explained in the right-hand side of the figure. With increasing sharpness of the indenter, the contact area between sample and indenter resembles its geometry better. This is in turn correlated to a decreased tendency to form edge cracks.

Figure reproduced from Yoshida et al. [66] under the Creative Commons Attribution 4.0 International License (CC BY 4.0).

Fig. 22. Scatter-plot of volume recovery ratio (V_R) as a function of Poisson's ratio (ν) for various oxide glasses. Data are taken from Refs. [33, 34, 38, 115, 116, 123, 125, 126, 129, 130, 136, 138, 149, 150]. The color of the data points refers to the content of B_2O_3 in trigonal coordination with oxygen normalized to the total content of B_2O_3 and SiO_2, i.e., $[B^{III}_2O_3]/([B_2O_3] + [SiO_2])$ ratio. The black data points correspond to glasses containing neither B_2O_3 nor SiO_2. V_R appears to decrease gradually with increasing ν. However, the glasses rich in trigonal boron are shifted to the right, suggesting that they are genera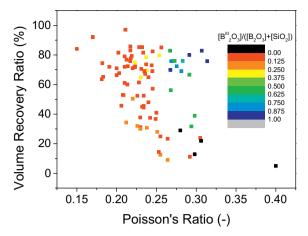lly more capable of densification. This is presumably controlled by their larger propensity to change the local atomic structure under loading [35].

7.2. Competing effects of bond strength and residual stress on crack initiation

Various researchers have attempted to correlate the propensity to densify with the resistance to indentation cracking in oxide glasses [32–34,63,136]. This is based on the idea that densification dissipates the energy supplied to the material during indentation, resulting in a lower residual stress upon unloading [31,32], which translates into a lower driving force for crack initiation. These considerations are based on Yoffe's stress field calculations [41] and later adjustments [34,63], with $1 - V_R$ used as a metric of the residual stress. However, while the calculations are capable of predicting the characteristic cracking pattern (mainly governed by ν), no predictive composition- or property-dependent model of CR exists [35]. The poor correlation between CR and V_R may be because the deformation mechanism at the atomic scale should be considered rather than simply the macroscopic volume change, as different structural rearrangements may lead to different extent of energy dissipation. Moreover, although Yoffe's stress field calculations [41] take residual stress into account (i.e., driving force for crack initiation), they do not contain any parameter quantifying the resistance to crack propagation. In other words, two glasses with the same set of properties (E, H, ν etc.) and same propensity to densify (i.e., identical V_R values) must necessarily exhibit the same CR value. However, if the toughness (i.e., the resistance to crack propagation) of the two glasses differs significantly, the proneness to form cracks should differ accordingly. This is in line with the conclusions drawn from MD simulations on Na−K aluminosilicate glasses [99], in which the resistance to indentation-induced fracture depends on two components: i) local fracture criterion, which is an intrinsic material property, depending largely on the chemical composition, and ii) stress evolution under indentation, depending on the indenter geometry or other extrinsic parameters. Additional supporting evidence for the importance of bond strength comes from the highly crack-resistant aluminate glasses containing no weak modifier bonds [151,152]. Although no V_R data is given for these glasses, the densification contribution is not expected to exceed that of, e.g., amorphous silica, with significantly worse resistance to indentation crack initiation.

In the following, we attempt to account for both the effects of driving force (residual stress) and activation barrier (bond strength) on

crack initiation. To do so, we first compute the molar dissociation energy content ($E_{D,glass}$) based on the dissociation energies and molar fractions of the constituent oxides for the glasses of interest (i.e., all oxide glasses where V_R and CR values are available [33,34,38,115,116,123–126,129,130,136,138,149,150]), as shown in Eq. (21).

$$E_{D,glass} = \sum x_{M_AO_B} E_{D,M_AO_B}, \tag{21}$$

where $x\_M_AO_B$ is the molar fraction of a given oxide, and E_{d, M_AO_B} is the dissociation energy of that oxide taken from Ref. [153]. $E_{D,glass}$ thus reflects the amount of energy per mole of glass unit needed to break all the bonds in a given network. For example, in a 20 mol% Na_2O – 80 mol % SiO_2 glass, the molar energy content can be calculated as in Eq. (22):

$$E_{D,glass} = 0.2 \cdot 1004 \frac{kJ}{mol} + 0.8 \cdot 1774 \frac{kJ}{mol} = 1620 \frac{kJ}{mol}. \tag{22}$$

Bond strength considerations have recently been successfully applied in the prediction of fracture toughness of oxide glasses [71]. Here, we use the product of V_R and $E_{D,glass}$ as a predictor for CR, as it contains both the proneness of the glass to dissipate energy and to resist crack initiation. As such, there is no physical meaning to this quantity, but it effectively presents which glasses pose a favorable balance between energy dissipation and crack initiation resistance.

There is a positive, exponential-like correlation between CR and $V_R E_{D,glass}$, although the data remain scattered (Fig. 23). However, the correlation is significantly improved compared to that of CR vs. V_R, as presented in Ref. [35]. The data scatter can be partially explained by the different experimental conditions used by different research groups (e.g., load or loading rate), which can influence the densification contribution relative to that of shear flow [64,135,143]. Furthermore, it should be noted that some studies only reported the critical load for generation of one and four cracks, respectively [36,125], rather than two as for the remainder of the data, causing these data points to deviate from the trend. Finally, it should be noted that in the prediction of fracture toughness, where propagation of cracks in oxide glasses is believed to follow the weak bonds of the network [71], the dissociation energy of the oxide bonds is normalized by density. This results in units of J/m^3 rather than J/mol as shown in Eq. (22). We argue the crack initiation resistance is related to the formation of a critical flaw, which can in principal initiate from the breakage of a single bond, i.e., bond density should not be important for prediction of CR. In this work, $E_{D,glass}$ was computed based on the average of all cation-oxygen bonds available in the glasses to simplify the calculation and to avoid unnecessary assumptions with regard to the most probable crack initiation. We expect that an improved prediction is possible in future work by accounting for the probability of breaking the different bonds as well as structural heterogeneities in the glasses.

8. Summary and perspectives

We have reviewed the open literature on the deformation mechanisms associated with indentation in oxide glasses. This subject is important from an engineering perspective, since a more in-depth understanding of how the deformation mechanism can be controlled, e.g., through adjusting the chemical composition, will facilitate the design of more damage-resilient glasses. Significant research efforts have already been directed towards this goal, and a general understanding of the link between the indentation deformation mechanism, associated structural changes, and the proneness to cracking has been established. For instance, promoting the ability to densify improves the crack resistance, since the elastic energy stored during loading can be dissipated through compaction of the material achieved through structural rearrangements in the glassy network. However, there is no one-to-one correlation between the ability to densify and crack resistance in oxide glasses, and multiple other factors need to be taken into account. This review has
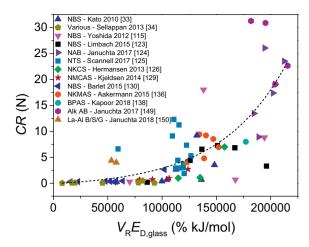
Fig. 23. Scatter plot of crack resistance (*CR*) as a function of the product of volume recovery ratio (*V*_R) and the molar glass dissociation energy (*E*_{D,glass}). Data from Refs. [33, 34, 115, 123–126, 129, 130, 136, 138, 149, 150]. Sellappan et al. [34] and Scannell et al. [125] report the critical load for generation of one and four cracks, respectively, rather than two corresponding to *CR*. The dashed line is a guide for the eye. The correlation suggests that higher *CR* can be obtained in glasses which exhibit a combination of many strong bonds and high propensity to densify.

summarized the current state of the art and reevaluated some of the existing data to provide new information and facilitate further research.

Many studies have focused on the quantification of the volume recovery ratio (V_R), which is a measure of how much of the supplied energy during loading can be dissipated through network densification. The available data suggests that there is a general negative correlation between Poisson's ratio (ν) and V_R. That is, oxide glasses with low ν usually exhibit high free volume fraction, facilitating densification, and high degree of cross-linking, increasing the resistance to shear deformation. Glasses with high ν tend to behave oppositely, since their low dimensionality facilitates shearing and lack of space between atoms hinders densification. However, the trend is rather scattered, and it is impossible to predict V_R based solely on ν, and we show that the chemical composition has a direct influence on the correlation. Boron-rich glasses tend to densify more easily than silicate glasses, which is probably attributed to the ability of trigonal boron atoms to increase their coordination number to four under compressive stress.

Higher ability to densify is often associated with higher resistance to indentation cracking. However, there appears to be a poor correlation between crack resistance (*CR*) and V_R. In this work, we argue that while the energy-dissipating network compaction has a large influence on *CR*, the strength of the bonds involved in the fracture process also needs to be considered. In other words, V_R can be used as an indicator of the residual stress driving the crack opening, while the bond strength can be seen as a resistance to crack initiation. Indeed, we find that the product of V_R and average bond strength (calculated from the dissociation energies of the oxides) exhibits a positive correlation with *CR*. Future work focusing on strong, yet easily compactible glassy networks might aid the discovery of even more crack-resistant oxide glasses.

Finally, we note that the vast majority of the reviewed work has focused on the densification contribution to the indentation-induced deformation. In our opinion, more light should be shed on the elastic recovery as well as the shear flow deformation modes. A better understanding of the structural features facilitating the initiation of shear flow, or a proper methodology to extract some quantifiable information regarding the shearing characteristics are desired.

References

[1] A.A. Griffith, The phenomena of rupture and flow in solids, Philos. Trans. R. Soc. London, Ser. A 221 (1921) 163–198, https://doi.org/10.2307/91192.

[2] A.H. Cotterell, Dislocation and Plastic Flow in Crystals, Clarendon Press, Oxford, 1953.

[3] E.W. Taylor, Plastic deformation of optical glass, Nature 163 (1949) 323, https://doi.org/10.1038/163323a0.

[4] J. Ainsworth, The diamond pyramid hardness of glass in relation to the strength and structure of glass. Part I. An investigation of the diamond pyramid hardness test applied to glass, J. Soc. Glas. Technol. 38 (1954) 479.

[5] W. Diehl, R. Schulze, Thermische, plastische nachwirkungen an vickerseindrücken in glas, Zeitschrift Für Angew. Math. Und Phys. 9 (1957) 251–253.

[6] J.H. Westbrook, Representative hardness values for fused quartz, Phys. Chem. Glasses 1 (1960) 32–36.

[7] G. Gehlhoff, M. Thomas, Die physikalischen eigenschaften der gläser in abhängigkeit von der zusammensetzung, Zeitschrift Für Tech. Phys. 6 (1926).

[8] E.B. Shand, Fracture velocity and fracture energy of glass in the fatigue range, J. Am. Ceram. Soc. 44 (1961) 21–26.

[9] G.R. Irwin, J.A. Kies, H.L. Smith, Fracture strengths relative to onset and arrest of crack propagation, Proc. ASTM, 1958, pp. 640–657.

[10] F.C. Roesler, Brittle fractures near equilibrium, Proc. Phys. Soc. Sect. B, 1956, p. 981.

[11] P.W. Bridgman, I. Simon, Effects of very high pressures on glass, J. Appl. Phys. 24 (1953) 405–413, https://doi.org/10.1063/1.1721294.

[12] P.W. Bridgman, The effect of pressure on the tensile properties of several metals and other materials, J. Appl. Phys. 24 (1953) 560–570, https://doi.org/10.1063/1.1721329.

[13] R.W. Douglas, Some comments on indentation tests on glass, J. Soc. Glas. Technol. 42 (1958) 145–157.

[14] D.M. Marsh, Plastic flow in glass, Proc. R. Soc. A Math. Phys. Eng. Sci. 279 (1964) 420–435, https://doi.org/10.1098/rspa.1964.0114.

[15] K.W. Peter, Densification and flow phenomena of glass in indentation experiments, J. Non-Cryst. Solids 5 (1970) 103–115, https://doi.org/10.1016/0022-3093(70)90188-2.

[16] M. Evers, Plastic deformation of glass with diamond indenters, Glastech. Ber. 40 (1967) 41–43.

[17] F.M. Ernsberger, Role of densification in deformation of glasses under point loading, J. Am. Ceram. Soc. 51 (1968) 545–547, https://doi.org/10.1111/j.1151-2916.1968.tb13318.x.

[18] J.D. Mackenzie, High-pressure effects on oxide glasses: II, subsequent heat treatment, J. Am. Ceram. Soc. 46 (1963) 470–476, https://doi.org/10.1111/j.1151-2916.1963.tb13777.x.

[19] J.E. Neely, J.D. Mackenzie, Hardness and low-temperature deformation of silica glass, J. Mater. Sci. 3 (1968) 603–609, https://doi.org/10.1007/bf00757906.

[20] K. Peter, Brittle fracture and microplasticity of glass in indentation experiments, Glastech. Ber. 37 (1964) 333–345.

[21] W.C. Oliver, G.M. Pharr, An improved technique for determining hardness and elastic modulus using load and displacement sensing indentation experiments, J. Mater. Res. 7 (1992) 1564–1583, https://doi.org/10.1557/JMR.1992.1564.

[22] M. Wada, H. Furukawa, K. Fujita, Crack resistance of glass on Vickers indentation, Proc. Xth Int. Congr. Glas, 1974, p. 39.

[23] B.R. Lawn, M.V. Swain, Microfracture beneath point indentations in brittle solids, J. Mater. Sci. 10 (1975) 113–122, https://doi.org/10.1007/BF00541038.

[24] A. Arora, D.B. Marshall, B.R. Lawn, M.V. Swain, Indentation deformation/fracture of normal and anomalous glasses, J. Non-Cryst. Solids 31 (1979) 415–428, https://doi.org/10.1016/0022-3093(79)90154-6.

[25] B.R. Lawn, A.G. Evans, D.B. Marshall, Elastic/plastic indentation damage in ceramics: the median/radial crack system, J. Am. Ceram. Soc. 63 (1980) 574–581, https://doi.org/10.1111/j.1151-2916.1980.tb10768.x.

[26] G.R. Anstis, P. Chantikul, B.R. Lawn, D.B. Marshall, A critical evaluation of indentation techniques for measuring fracture toughness: I, direct crack measurements, J. Am. Ceram. Soc. 64 (1981) 533–538, https://doi.org/10.1111/j.1151-2916.1981.tb10320.x.

[27] K. Niihara, R. Morena, D.P.H. Hasselman, Evaluation of Kic of brittle solids by the indentation method with low crack-to-indent ratios, J. Mater. Sci. Lett. 1 (1982) 13–16 https://link.springer.com/content/pdf/10.1007/BF00724706.pdf , Accessed date: 19 April 2018.

[28] M. Sakai, R.C. Bradt, Fracture toughness testing of brittle materials, Int. Mater. Rev. 38 (1993) 53–78, https://doi.org/10.1179/imr.1993.38.2.53.

[29] R. Morrell, Fracture toughness testing for advanced technical ceramics: internationally agreed good practice, Adv. Appl. Ceram. 105 (2006) 88–98, https://doi.org/10.1179/174367606X84422.

[30] G.D. Quinn, R.C. Bradt, On the Vickers indentation fracture toughness test, J. Am. Ceram. Soc. 90 (2007) 673–680, https://doi.org/10.1111/j.1551-2916.2006.

01482.x.

[31] J. Sehgal, S. Ito, A new low-brittleness glass in the soda-lime-silica glass family, J. Am. Ceram. Soc. 81 (1998) 2485–2488, https://doi.org/10.1111/j.1151-2916.1998.tb02649.x.

[32] Y. Kato, H. Yamazaki, S. Yoshida, J. Matsuoka, Effect of densification on crack initiation under Vickers indentation test, J. Non-Cryst. Solids 356 (2010) 1768–1773, https://doi.org/10.1016/j.jnoncrysol.2010.07.015.

[33] Y. Kato, H. Yamazaki, Y. Kubo, S. Yoshida, J. Matsuoka, T. Akai, Effect of B_2O_3 content on crack initiation under Vickers indentation test, J. Ceram. Soc. Jpn. 118 (2010) 792–798, https://doi.org/10.2109/jcersj2.118.792.

[34] P. Sellappan, T. Rouxel, F. Celarie, E. Becker, P. Houizot, R. Conradt, Composition dependence of indentation deformation and indentation cracking in glass, Acta Mater. 61 (2013) 5949–5965, https://doi.org/10.1016/j.actamat.2013.06.034.

[35] K. Januchta, R.E. Youngman, A. Goel, M. Bauchy, S.L. Logunov, S.J. Rzoska, M. Bockowski, L.R. Jensen, M.M. Smedskjaer, Discovery of ultra-crack-resistant oxide glasses with adaptive networks, Chem. Mater. 29 (2017) 5865–5876, https://doi.org/10.1021/acs.chemmater.7b00921.

[36] H. Hertz, On the contact of elastic solids, J. Für Die Reine Und Angew. Math. 92 (1881) 156–171.

[37] A.K. Varshneya, Stronger glass products: lessons learned and yet to be learned, Int. J. Appl. Glas. Sci. 9 (2018) 140–155, https://doi.org/10.1111/ijag.12341.

[38] S. Yoshida, J.-C. Sangleboeuf, T. Rouxel, Quantitative evaluation of indentation-induced densification in glass, J. Mater. Res. 20 (2005) 3404–3412, https://doi.org/10.1557/jmr.2005.0418.

[39] T. Rouxel, H. Ji, J.P. Guin, F. Augereau, B. Rufflé, Indentation deformation mechanism in glass: densification versus shear flow, J. Appl. Phys. 107 (2010) 94903, , https://doi.org/10.1063/1.3407559.

[40] V. Keryvin, S. Gicquel, L. Charleux, J.P. Guin, M. Nivard, J.C. Sangleboeuf, Densification as the only mechanism at stake during indentation of silica glass? Key Eng. Mater. 606 (2014) 53–60, https://doi.org/10.4028/www.scientific.net/KEM.606.53.

[41] E.H. Yoffe, Elastic stress fields caused by indenting brittle materials, Philos. Mag. A 46 (1982) 617–628, https://doi.org/10.1080/01418618208236917.

[42] M. Bobji, S. Biswas, Estimation of hardness by nanoindentation of rough surfaces, J. Mater. Res. 13 (1998) 3227–3233 http://eprints.iisc.ernet.in/1395/ , Accessed date: 30 April 2018.

[43] D. Tabor, Microindentation techniques in materials science, in: P.J. Blau, B.R. Lawn (Eds.), Microindentation Tech. Mater. Sci, vol. 889, ASTM-STP, 1986, p. 129.

[44] J.T. Hagan, Shear deformation under pyramidal indentations in soda-lime glass, J. Mater. Sci. 15 (1980) 1417–1424, https://doi.org/10.1007/BF00752121.

[45] R. Chakraborty, A. Dey, A.K. Mukhopadhyay, Loading rate effect on nanohardness of soda-lime-silica glass, Metall. Mater. Trans. A 41 (2010) 1301–1312, https://doi.org/10.1007/s11661-010-0176-8.

[46] D.A. Kilymis, J.-M. Delaye, Deformation mechanisms during nanoindentation of sodium borosilicate glasses of nuclear interest, J. Chem. Phys. 141 (2014) 14504, , https://doi.org/10.1063/1.4885850.

[47] A.G. Evans, T.R. Wilshaw, Quasi-static solid particle damage in brittle solids—I. Observations analysis and implications, Acta Metall. 24 (1976) 939–956, https://doi.org/10.1016/0001-6160(76)90042-0.

[48] K. Philips, G.M. Crimes, T.R. Wilshaw, On the mechanism of material removal by free abrasive grinding of glass and fused silica, Wear 41 (1977) 327–350, https://doi.org/10.1016/0043-1648(77)90012-6.

[49] J.T. Hagan, M.V. Swain, The origin of median and lateral cracks around plastic indents in brittle materials, J. Phys. D. Appl. Phys. 11 (1978) 2091–2102, https://doi.org/10.1088/0022-3727/11/15/007.

[50] J.T. Hagan, Cone cracks around Vickers indentations in fused silica glass, J. Mater. Sci. 14 (1979) 462–466, https://doi.org/10.1007/BF00589840.

[51] J.T. Hagan, Micromechanics of crack nucleation during indentations, J. Mater. Sci. 14 (1979) 2975–2980, https://doi.org/10.1007/BF00611482.

[52] J.H. Lee, Y.F. Gao, K.E. Johanns, G.M. Pharr, Cohesive interface simulations of indentation cracking as a fracture toughness measurement method for brittle materials, Acta Mater. 60 (2012) 5448–5467, https://doi.org/10.1016/J.ACTAMAT.2012.07.011.

[53] M. Jebahi, D. André, F. Dau, J.-L. Charles, I. Iordanoff, Simulation of Vickers indentation of silica glass, J. Non-Cryst. Solids 378 (2013) 15–24, https://doi.org/10.1016/J.JNONCRYSOL.2013.06.007.

[54] S. Bruns, K.E. Johanns, H.U.R. Rehman, G.M. Pharr, K. Durst, Constitutive modeling of indentation cracking in fused silica, J. Am. Ceram. Soc. 100 (2017) 1928–1940, https://doi.org/10.1111/jace.14734.

[55] S. Spinner, Elastic moduli of glasses at elevated temperatures by a dynamic method, J. Am. Ceram. Soc. 39 (1956) 113–118, https://doi.org/10.1111/j.1151-2916.1956.tb15634.x.

[56] S.M. Wiederhorn, Fracture surface energy of glass, J. Am. Ceram. Soc. 52 (1969) 99–105, https://doi.org/10.1111/j.1151-2916.1969.tb13350.x.

[57] R. Brückner, Properties and structure of vitreous silica. I, J. Non-Cryst. Solids 5 (1970) 123–175, https://doi.org/10.1016/0022-3093(70)90190-0.

[58] R.F. Cook, G.M. Pharr, Direct observation and analysis of indentation cracking in glasses and ceramics, J. Am. Ceram. Soc. 73 (1990) 787–817, https://doi.org/10.1111/j.1151-2916.1990.tb05119.x.

[59] C.R. Kurkjian, G.W. Kammlott, M.M. Chaudhri, Indentation behavior of soda-lime silica glass, fused silica, and single-crystal quartz at liquid nitrogen temperature, J. Am. Ceram. Soc. 78 (1995) 737–744, https://doi.org/10.1111/j.1151-2916.1995.tb08241.x.

[60] S. Yoshida, S. Isono, J. Matsuoka, N. Soga, Shrinkage behavior of knoop indentations in silica and soda-lime-silica glasses, J. Am. Ceram. Soc. 84 (2001)

2141–2143, https://doi.org/10.1111/j.1151-2916.2001.tb00976.x.

[61] A. Koike, M. Tomozawa, IR investigation of density changes of silica glass and soda-lime silicate glass caused by microhardness indentation, J. Non-Cryst. Solids 353 (2007) 2318–2327, https://doi.org/10.1016/j.jnoncrysol.2007.04.006.

[62] G. Kermouche, E. Barthel, D. Vandembroucq, P. Dubujet, Mechanical modelling of indentation-induced densification in amorphous silica, Acta Mater. 56 (2008) 3222–3228, https://doi.org/10.1016/J.ACTAMAT.2008.03.010.

[63] T. Rouxel, Driving force for indentation cracking in glass: composition, pressure and temperature dependence, Philos. Transact. A Math. Phys. Eng. Sci. 373 (2015), https://doi.org/10.1098/rsta.2014.0140.

[64] T.M. Gross, J.J. Price, Vickers indentation cracking of ion-exchanged glasses: quasi-static vs. dynamic contact, Front. Mater. Sci. 4 (2017) 4, , https://doi.org/10.3389/fmats.2017.00004.

[65] T.K. Bechgaard, J.C. Mauro, M.M. Smedskjaer, Time and humidity dependence of indentation cracking in aluminosilicate glasses, J. Non-Cryst. Solids 491 (2018) 64–70, https://doi.org/10.1016/J.JNONCRYSOL.2018.04.009.

[66] S. Yoshida, K. Wada, T. Fujimura, A. Yamada, M. Kato, J. Matsuoka, N. Soga, Evaluation of sinking-in and cracking behavior of soda-lime glass under varying angle of trigonal pyramid indenter, Front. Mater. Sci. 3 (2016) 54, , https://doi.org/10.3389/fmats.2016.00054.

[67] A. Pönitzsch, M. Nofz, L. Wondraczek, J. Deubener, Bulk elastic properties, hardness and fatigue of calcium aluminosilicate glasses in the intermediate-silica range, J. Non-Cryst. Solids 434 (2016) 1–12, https://doi.org/10.1016/J.JNONCRYSOL.2015.12.002.

[68] D.K. Shetty, I.G. Wright, P.N. Mincer, A.H. Clauer, Indentation fracture of WC-Co cermets, J. Mater. Sci. 20 (1985) 1873–1882, https://doi.org/10.1007/BF00555296.

[69] T. Miyoshi, N. Sagwa, T. Sasa, Study of evaluation for fracture toughness of structural ceramics, Trans. Jpn. Soc. Mech. Eng., A 51A (1985) 2489–2497.

[70] C. Relias, D. Ngai, Indentation fracture toughness: a review and application, Am. Ceram. Soc. Bull. 97 (2018) 34–37.

[71] T. Rouxel, S. Yoshida, The fracture toughness of inorganic glasses, J. Am. Ceram. Soc. 100 (2017) 4374–4396, https://doi.org/10.1111/jace.15108.

[72] T.M. Gross, M. Tomozawa, Indentation-induced microhardness changes in glasses: possible fictive temperature increase caused by plastic deformation, J. Non-Cryst. Solids 354 (2008) 4056–4062, https://doi.org/10.1016/j.jnoncrysol.2008.05.042.

[73] A. Perriot, D. Vandembroucq, E. Barthel, V. Martinez, L. Grosvalet, C. Martinet, B. Champagnon, Raman microspectroscopic characterization of amorphous silica plastic behavior, J. Am. Ceram. Soc. 89 (2006) 596–601, https://doi.org/10.1111/j.1551-2916.2005.00747.x.

[74] T. To, F. Célarié, C. Roux-Langlois, A. Bazin, Y. Gueguen, H. Orain, M. Le Fur, V. Burgaud, T. Rouxel, Fracture toughness, fracture energy and slow crack growth of glass as investigated by the Single-Edge Precracked Beam (SEPB) and Chevron-Notched Beam (CNB) methods, Acta Mater. 146 (2018) 1–11, https://doi.org/10.1016/J.ACTAMAT.2017.11.056.

[75] T. Rouxel, J.-C. Sangleboeuf, C. Moysan, B. Truffin, Indentation topometry in glasses by atomic force microscopy, J. Non-Cryst. Solids 344 (2004) 26–36, https://doi.org/10.1016/J.JNONCRYSOL.2004.07.020.

[76] H. Sawasato, S. Yoshida, T. Suguwara, Y. Miura, J. Matsuoka, Relaxation behaviors of Vickers indentations in soda-lime glass, J. Ceram. Soc. Jpn. 116 (2008) 864–868, https://doi.org/10.2109/jcersj2.116.864.

[77] C.A. Angell, Formation of glasses from liquids and biopolymers, Source Sci. New Ser. 267 (1995) 1924–1935 http://www.jstor.org/stable/2886440 , Accessed date: 26 July 2017.

[78] Y.-F. Niu, K. Han, J.-P. Guin, Locally enhanced dissolution rate as a probe for nanocontact-induced densification in oxide glasses, Langmuir 28 (2012) 10733–10740, https://doi.org/10.1021/la300972j.

[79] J.-P. Guin, V. Keryvin, L. Charleux, K. Han, J.-C. Sangleboeuf, M. Ferry, A chemical dissolution technique for challenging existing constitutive models of the densification process beneath an indentation imprint in amorphous silica, http://arxiv.org/abs/1601.06492, (2016) , Accessed date: 28 July 2017.

[80] B. Hehlen, Inter-tetrahedra bond angle of permanently densified silicas extracted from their Raman spectra, J. Phys. Condens. Matter 22 (2010) 25401, , https://doi.org/10.1088/0953-8984/22/2/025401.

[81] T. Deschamps, C. Martinet, J.L. Bruneel, B. Champagnon, Soda-lime silicate glass under hydrostatic pressure and indentation: a micro-Raman study, J. Phys. Condens. Matter 23 (2011) 35402, , https://doi.org/10.1088/0953-8984/23/3/035402.

[82] H. Sugiura, T. Yamadaya, Raman scattering in silica glass in the permanent densification region, J. Non-Cryst. Solids 144 (1992) 151–158, https://doi.org/10.1016/S0022-3093(05)80395-3.

[83] R.A.B. Devine, Ion implantation- and radiation-induced structural modifications in amorphous SiO_2, J. Non-Cryst. Solids 152 (1993) 50–58, https://doi.org/10.1016/0022-3093(93)90443-2.

[84] D.-L. Kim, M. Tomozawa, Fictive temperature of silica glass optical fibers – re-examination, J. Non-Cryst. Solids 286 (2001) 132–138, https://doi.org/10.1016/S0022-3093(01)00505-1.

[85] H. Tran, S. Clément, R. Vialla, D. Vandembroucq, B. Rufflé, Micro-Brillouin spectroscopy mapping of the residual density field induced by Vickers indentation in a soda-lime silicate glass, Appl. Phys. Lett. 100 (2012) 231901, , https://doi.org/10.1063/1.4725488.

[86] A. Perriot, E. Barthel, G. Kermouche, G. Quérel, D. Vandembroucq, On the plastic deformation of soda-lime glass – a Cr^{3+} luminescence study of densification, Philos. Mag. 91 (2011) 1245–1255, https://doi.org/10.1080/14786435.2010.491808.

[87] G. Quérel, B. Reynard, High-pressure luminescence spectroscopy of transition

elements: experimental setup and preliminary results on Cr^{3+} in silicate glasses, Chem. Geol. 128 (1996) 65–75, https://doi.org/10.1016/0009-2541(95)00163-8.

[88] M. Imaoka, I. Yasui, Finite element analysis of indentation on glass, J. Non-Cryst. Solids 22 (1976) 315–329, https://doi.org/10.1016/0022-3093(76)90062-4.

[89] I. Yasui, M. Imaoka, Finite element analysis of indentation on glass(II), J. Non-Cryst. Solids 50 (1982) 219–232, https://doi.org/10.1016/0022-3093(82)90269-1.

[90] K. Xin, J.C. Lambropoulos, Densification of fused silica: effects on nanoindentation, in: A.J. Marker, IIIE.G. Arthurs (Eds.), Inorg. Opt. Mater. II, International Society for Optics and Photonics, 2000, pp. 112–121, , https://doi.org/10.1117/12.405275.

[91] V. Keryvin, J.-X. Meng, S. Gicquel, J.-P. Guin, L. Charleux, J.-C. Sanglebœuf, P. Pilvin, T. Rouxel, G. Le Quilliec, Constitutive modeling of the densification process in silica glass under hydrostatic compression, Acta Mater. 62 (2014) 250–257, https://doi.org/10.1016/j.actamat.2013.07.067.

[92] V. Keryvin, L. Charleux, R. Hin, J.-P. Guin, J.-C. Sanglebœuf, Mechanical behaviour of fully densified silica glass under Vickers indentation, Acta Mater. 129 (2017) 492–499, https://doi.org/10.1016/J.ACTAMAT.2017.03.008.

[93] G. Molnár, P. Ganster, A. Tanguy, E. Barthel, G. Kermouche, Densification dependent yield criteria for sodium silicate glasses - an atomistic simulation approach, Acta Mater. 111 (2016), https://doi.org/10.1016/j.actamat.2016.03.053.

[94] D. André, M. Jebahi, I. Iordanoff, J. Charles, J. Néauport, Using the discrete element method to simulate brittle fracture in the indentation of a silica glass with a blunt indenter, Comput. Methods Appl. Mech. Eng. 265 (2013) 136–147, https://doi.org/10.1016/j.CMA.2013.06.008.

[95] A. Pedone, G. Malavasi, M.C. Menziani, A.N. Cormack, U. Segre, A new self-consistent empirical interatomic potential model for oxides, silicates, and silica-based glasses, J. Phys. Chem. B 110 (2006) 11780–11795, https://doi.org/10.1021/JP0611018.

[96] B.W.H. van Beest, G.J. Kramer, R.A. van Santen, Force fields for silicas and aluminophosphates based on *ab initio* calculations, Phys. Rev. Lett. 64 (1990) 1955–1958, https://doi.org/10.1103/PhysRevLett.64.1955.

[97] F. Yuan, L. Huang, Brittle to ductile transition in densified silica glass, Sci. Rep. 4 (2014) 5035, , https://doi.org/10.1038/srep05035.

[98] Y. Yu, M. Wang, N.M. Anoop Krishnan, M.M. Smedskjaer, K. Deenamma Varghese, J.C. Mauro, M. Balonis, M. Bauchy, Hardness of silicate glasses: atomic-scale origin of the mixed modifier effect, J. Non-Cryst. Solids 489 (2018) 16–21, https://doi.org/10.1016/J.JNONCRYSOL.2018.03.015.

[99] J. Luo, K.D. Varghese, A. Tandia, G. Hu, J.C. Mauro, Crack nucleation criterion and its application to impact indentation in glasses, Sci. Rep. 6 (2016) 23720, , https://doi.org/10.1038/srep23720.

[100] J. Luo, P.J. Lezzi, K.D. Varghese, A. Tandia, J.T. Harris, T.M. Gross, J.C. Mauro, Competing indentation deformation mechanisms in glass using different strengthening methods, Front. Mater. Sci. 3 (2016) 52, , https://doi.org/10.3389/fmats.2016.00052.

[101] R.J. Hemley, H.K. Mao, P.M. Bell, B.O. Mysen, Raman spectroscopy of SiO_2 glass at high pressure, Phys. Rev. Lett. 57 (1986) 747–750, https://doi.org/10.1103/PhysRevLett.57.747.

[102] J.C. Lambropoulos, S. Xu, T. Fang, Constitutive law for the densification of fused silica, with applications to polishing and microgrinding, J. Am. Ceram. Soc. 79 (1996) 1441–1452, https://doi.org/10.1111/j.1151-2916.1996.tb08748.x.

[103] L. Huang, J. Kieffer, Amorphous-amorphous transitions in silica glass. I. Reversible transitions and thermomechanical anomalies, Phys. Rev. B 69 (2004) 224203, , https://doi.org/10.1103/PhysRevB.69.224203.

[104] B. Champagnon, C. Martinet, M. Boudelle, D. Vouagner, C. Coussa, T. Deschamps, L. Grosvalet, High pressure elastic and plastic deformations of silica: in situ diamond anvil cell Raman experiments, J. Non-Cryst. Solids 354 (2008) 569–573, https://doi.org/10.1016/J.JNONCRYSOL.2007.07.079.

[105] T. Rouxel, H. Ji, T. Hammouda, A. Moréac, Poisson's ratio and the densification of glass under high pressure, Phys. Rev. Lett. 100 (2008) 225501, , https://doi.org/10.1103/PhysRevLett.100.225501.

[106] F.L. Galeener, Planar rings in glasses, Solid State Commun. 44 (1982) 1037–1040, https://doi.org/10.1016/0038-1098(82)90329-5.

[107] B. Champagnon, C. Chemarin, E. Duval, R. Le Parc, Glass structure and light scattering, J. Non-Cryst. Solids 274 (2000) 81–86, https://doi.org/10.1016/S0022-3093(00)00207-6.

[108] R. Le Parc, B. Champagnon, P. Guenot, S. Dubois, Thermal annealing and density fluctuations in silica glass, J. Non-Cryst. Solids 293–295 (2001) 366–369, https://doi.org/10.1016/S0022-3093(01)00835-3.

[109] D.A. Kilymis, J.M. Delaye, Nanoindentation of pristine and disordered silica: molecular dynamics simulations, J. Non-Cryst. Solids 382 (2013) 87–94, https://doi.org/10.1016/J.JNONCRYSOL.2013.10.013.

[110] M. Guerette, M.R. Ackerson, J. Thomas, F. Yuan, E. Bruce Watson, D. Walker, L. Huang, Structure and properties of silica glass densified in cold compression and hot compression, Sci. Rep. 5 (2015), https://doi.org/10.1038/srep15343.

[111] C. Martinet, A. Kassir-Bodon, T. Deschamps, A. Cornet, S. Le Floch, V. Martinez, B. Champagnon, Permanently densified SiO_2 glasses: a structural approach, J. Phys. Condens. Matter 27 (2015) 325401, , https://doi.org/10.1088/0953-8984/27/32/325401.

[112] X.X. Xue, J.F. Stebbins, M. Kanzaki, P.F. McMillan, B. Poe, Pressure-induced silicon coordination and tetrahedral structural changes in alkali oxide-silica melts up to 12 GPa: NMR, Raman, and infrared spectroscopy, Am. Mineral. 76 (1991) 8–26 https://okayama.pure.elsevier.com/en/publications/pressure-induced-silicon-coordination-and-tetrahedral-structural- , Accessed date: 19 April 2018.

[113] Y. Kato, H. Yamazaki, S. Yoshida, J. Matsuoka, M. Kanzaki, Measurements of density distribution around Vickers indentation on commercial aluminoborosilicate and soda-lime silicate glasses by using micro Raman spectroscopy, J. Non-Cryst. Solids (2012), https://doi.org/10.1016/j.jnoncrysol.2012.04.035.

[114] A. Winterstein-Beckmann, D. Möncke, D. Palles, E.I. Kamitsos, L. Wondraczek, A Raman-spectroscopic study of indentation-induced structural changes in technical alkali-borosilicate glasses with varying silicate network connectivity, J. Non-Cryst. Solids 405 (2014), https://doi.org/10.1016/j.jnoncrysol.2014.09.020.

[115] S. Yoshida, Y. Nishikubo, A. Konno, T. Sugawara, Y. Miura, J. Matsuoka, Fracture- and indentation-induced structural changes of sodium borosilicate glasses, Int. J. Appl. Glas. Sci. 3 (2012) 3–13, https://doi.org/10.1111/j.2041-1294.2011.00077.x.

[116] S. Yoshida, Y. Hayashi, A. Konno, T. Sugawara, Y. Miura, J. Matsuoka, Indentation induced densification of sodium borate glasses, Phys. Chem. Glasses Eur. J. Glass Sci. Technol. B 50 (2009) 63–70 http://www.ingentaconnect.com/content/sgt/ejgst/2009/00000050/00000001/art00016 , Accessed date: 28 July 2017.

[117] S.K. Lee, P.J. Eng, H.-K. Mao, Y. Meng, M. Newville, M.Y. Hu, J. Shu, Probing of bonding changes in B_2O_3 glasses at high pressure with inelastic X-ray scattering, Nat. Mater. 4 (2005) 851, https://doi.org/10.1038/nmat1511.

[118] T.M. Gross, Deformation and cracking behavior of glasses indented with diamond tips of various sharpness, J. Non-Cryst. Solids 358 (2012) 3445–3452, https://doi.org/10.1016/j.jnoncrysol.2012.01.052.

[119] T.M. Gross, J. Wu, D.E. Baker, J.J. Price, R. Yongsunthon, Crack-resistant glass with high shear band density, J. Non-Cryst. Solids 494 (2018) 13–20, https://doi.org/10.1016/j.jnoncrysol.2018.04.048.

[120] A. Kassir-Bodon, T. Deschamps, C. Martinet, B. Champagnon, J. Teisseire, G. Kermouche, Raman mapping of the indentation-induced densification of a soda-lime-silicate glass, Int. J. Appl. Glas. Sci. 3 (2012) 29–35, https://doi.org/10.1111/J.2041-1294.2012.00078.X.

[121] H. Ji, V. Keryvin, T. Rouxel, T. Hammouda, Densification of window glass under very high pressure and its relevance to Vickers indentation, Scr. Mater. 55 (2006) 1159–1162, https://doi.org/10.1016/j.scriptamat.2006.08.038.

[122] T. Rouxel, Elastic properties and short-to medium-range order in glasses, J. Am. Ceram. Soc. 90 (2007) 3019–3039, https://doi.org/10.1111/j.1551-2916.2007.01945.x.

[123] R. Limbach, A. Winterstein-Beckmann, J. Dellith, D. Möncke, L. Wondraczek, Plasticity, crack initiation and defect resistance in alkali-borosilicate glasses: from normal to anomalous behavior, J. Non-Cryst. Solids 417–418 (2015) 15–27, https://doi.org/10.1016/j.jnoncrysol.2015.02.019.

[124] K. Januchta, R.E. Youngman, A. Goel, M. Bauchy, S.J. Rzoska, M. Bockowski, M.M. Smedskjaer, Structural origin of high crack resistance in sodium aluminoborate glasses, J. Non-Cryst. Solids 460 (2017) 54–65, https://doi.org/10.1016/j.jnoncrysol.2017.01.019.

[125] G. Scannell, D. Laille, F. Célarié, L. Huang, T. Rouxel, Interaction between deformation and crack initiation under Vickers indentation in $Na_2O–TiO_2–SiO_2$ glasses, Front. Mater. Sci. 4 (2017) 6, , https://doi.org/10.3389/fmats.2017.00006.

[126] C. Hermansen, J. Matsuoka, S. Yoshida, H. Yamazaki, Y. Kato, Y.Z. Yue, Densification and plastic deformation under microindentation in silicate glasses and the relation to hardness and crack resistance, J. Non-Cryst. Solids 364 (2013), https://doi.org/10.1016/j.jnoncrysol.2012.12.047.

[127] G.N. Greaves, EXAFS and the structure of glass, J. Non-Cryst. Solids 71 (1985) 203–217, https://doi.org/10.1016/0022-3093(85)90289-3.

[128] J. Kjeldsen, M.M. Smedskjaer, J.C. Mauro, Y. Yue, On the origin of the mixed alkali effect on indentation in silicate glasses, J. Non-Cryst. Solids 406 (2014), https://doi.org/10.1016/j.jnoncrysol.2014.09.036.

[129] J. Kjeldsen, M.M. Smedskjaer, J.C. Mauro, Y. Yue, Hardness and incipient plasticity in silicate glasses: origin of the mixed modifier effect, Appl. Phys. Lett. 104 (2014) 51913, , https://doi.org/10.1063/1.4864400.

[130] M. Barlet, J.M. Delaye, T. Charpentier, M. Gennisson, D. Bonamy, T. Rouxel, C.L. Rountree, Hardness and toughness of sodium borosilicate glasses via Vickers's indentations, J. Non-Cryst. Solids 417–418 (2015) 1–15, https://doi.org/10.1016/j.jnoncrysol.2015.02.005.

[131] D. Manara, A. Grandjean, D.R. Neuville, Structure of borosilicate glasses and melts: a revision of the Yun, Bray and Dell model, J. Non-Cryst. Solids 355 (2009) 2528–2531, https://doi.org/10.1016/J.JNONCRYSOL.2009.08.033.

[132] R. Gresch, W. Müller-Warmuth, H. Dutz, ^{11}B and ^{27}Al NMR studies of glasses in the system $Na_2O-B_2O_3-Al_2O_3$ ("NABAL"), J. Non-Cryst. Solids 21 (1976) 31–40, https://doi.org/10.1016/0022-3093(76)90088-0.

[133] S. Striepe, J. Deubener, M. Potuzak, M.M. Smedskjaer, A. Matthias, Thermal history dependence of indentation induced densification in an aluminosilicate glass, J. Non-Cryst. Solids 445–446 (2016) 34–39, https://doi.org/10.1016/j.jnoncrysol.2016.04.046.

[134] P. Malchow, K.E. Johanns, D. Möncke, S. Korte-Kerzel, L. Wondraczek, K. Durst, Composition and cooling-rate dependence of plastic deformation, densification, and cracking in sodium borosilicate glasses during pyramidal indentation, J. Non-Cryst. Solids 419 (2015), https://doi.org/10.1016/j.jnoncrysol.2015.03.020.

[135] C. Zehnder, S. Bruns, J.-N. Peltzer, K. Durst, S. Korte-Kerzel, D. Möncke, Influence of cooling rate on cracking and plastic deformation during impact and indentation of borosilicate glasses, Front. Mater. Sci. 4 (2017) 5, , https://doi.org/10.3389/fmats.2017.00005.

[136] K.G. Aakermann, K. Januchta, J.A.L. Pedersen, M.N. Svenson, S.J. Rzoska, M. Bockowski, J.C. Mauro, M. Guerette, L. Huang, M.M. Smedskjaer, Indentation deformation mechanism of isostatically compressed mixed alkali aluminosilicate glasses, J. Non-Cryst. Solids 426 (2015) 175–183, https://doi.org/10.1016/j.jnoncrysol.2015.06.028.

[137] S. Kapoor, L. Wondraczek, M.M. Smedskjaer, Pressure-induced densification of

oxide glasses at the glass transition, Front. Mater. Sci. 4 (2017) 1, , https://doi.org/10.3389/fmats.2017.00001.

[138] S. Kapoor, K. Januchta, R.E. Youngman, X. Guo, J.C. Mauro, M. Bauchy, S.J. Rzoska, M. Bockowski, L.R. Jensen, M.M. Smedskjaer, Combining high hardness and crack resistance in mixed network glasses through high-temperature densification, Phys. Rev. Mater. 2 (2018) 63603, , https://doi.org/10.1103/PhysRevMaterials.2.063603.

[139] A. Koike, S. Akiba, T. Sakagami, K. Hayashi, S. Ito, Difference of cracking behavior due to Vickers indentation between physically and chemically tempered glasses, J. Non-Cryst. Solids 358 (2012) 3438–3444, https://doi.org/10.1016/J.JNONCRYSOL.2012.02.020.

[140] A. Dey, R. Chakraborty, A.K. Mukhopadhyay, Enhancement in nanohardness of soda–lime–silica glass, J. Non-Cryst. Solids 357 (2011) 2934–2940, https://doi.org/10.1016/J.JNONCRYSOL.2011.03.036.

[141] R. Limbach, B.P. Rodrigues, L. Wondraczek, Strain-rate sensitivity of glasses, J. Non-Cryst. Solids 404 (2014) 124–134, https://doi.org/10.1016/J.JNONCRYSOL.2014.08.023.

[142] O. Shikimaka, D. Grabco, B.A. Sava, M. Elisa, L. Boroica, E. Harea, C. Pyrtsac, A. Prisacaru, Z. Barbos, Densification contribution as a function of strain rate under indentation of terbium-doped aluminophosphate glass, J. Mater. Sci. 51 (2016) 1409–1417, https://doi.org/10.1007/s10853-015-9460-8.

[143] Y. Kato, H. Yamazaki, S. Itakura, S. Yoshida, J. Matsuoka, Load dependence of densification in glass during Vickers indentation test, J. Ceram. Soc. Jpn. 119 (2011) 110–115, https://doi.org/10.2109/jcersj2.119.110.

[144] S. Yoshida, H. Sawasato, T. Sugawara, Y. Miura, J. Matsuoka, Effects of indenter geometry on indentation-induced densification of soda-lime glass, J. Mater. Res. 25 (2010) 2203–2211, https://doi.org/10.1557/jmr.2010.0287.

[145] D.-H. Lee, I.-C. Choi, M.-Y. Seok, Y. Zhao, J.-A. Lee, J. Jang, Strain-dependent plasticity evolution of window glass, J. Am. Ceram. Soc. 98 (2015) 186–189, https://doi.org/10.1111/jace.13266.

[146] S. Yoshida, M. Kato, A. Yokota, S. Sasaki, A. Yamada, J. Matsuoka, N. Soga, C.R. Kurkjian, Direct observation of indentation deformation and cracking of silicate glasses, J. Mater. Res. 30 (2015) 2291–2299, https://doi.org/10.1557/jmr.2015.214.

[147] M.N. Svenson, T.K. Bechgaard, S.D. Fuglsang, R.H. Pedersen, A.O. Tjell, M.B. Østergaard, R.E. Youngman, J.C. Mauro, S.J. Rzoska, M. Bockowski, M.M. Smedskjaer, Composition-structure-property relations of compressed borosilicate glasses, Phys. Rev. Appl. 2 (2014), https://doi.org/10.1103/PhysRevApplied.2.024006.

[148] S.K. Lee, K. Mibe, Y. Fei, G.D. Cody, B.O. Mysen, Structure of B_2O_3 Glass at High Pressure: A ^{11}B Solid-State NMR Study, Phys. Rev. Lett. 94 (2005) 165507, https://doi.org/10.1103/PhysRevLett.94.165507.

[149] K. Januchta, M. Bauchy, R.E. Youngman, S.J. Rzoska, M. Bockowski, M.M. Smedskjaer, Modifier field strength effects on densification behavior and mechanical properties of alkali aluminoborate glasses, Phys. Rev. Mater. 1 (2017) 63603, , https://doi.org/10.1103/PhysRevMaterials.1.063603.

[150] K. Januchta, R. Sun, L. Huang, M. Bockowski, S.J. Rzoska, L.R. Jensen, M.M. Smedskjaer, Deformation and cracking behavior of La_2O_3-doped oxide glasses with high Poisson's ratio, J. Non-Cryst. Solids 494 (2018) 86–93, https://doi.org/10.1016/j.jnoncrysol.2018.04.058.

[151] G.A. Rosales-Sosa, A. Masuno, Y. Higo, H. Inoue, Crack-resistant Al_2O_3-SiO_2 glasses, Sci. Rep. 6 (2016) 23620, , https://doi.org/10.1038/srep23620.

[152] G.A. Rosales-Sosa, A. Masuno, Y. Higo, Y. Watanabe, H. Inoue, Effect of rare-earth ion size on elasticity and crack initiation in rare-earth aluminate glasses, J. Am. Ceram. Soc. 101 (2018) 5030–5036, https://doi.org/10.1111/jace.15760.

[153] K.-H. Sun, Fundamental condition of glass formation, J. Am. Ceram. Soc. 30 (1947) 277–281, https://doi.org/10.1111/j.1151-2916.1947.tb19654.x.